R7 photoreceptor axon targeting requires matching levels of the Lost and found protein in R7 and its synaptic partners

Jessica Douthit[1,4], Ariel Hairston[1,4], Gina Lee[1], Carolyn A. Morrison[1], Isabel Holguera[2] and Jessica E. Treisman[1,3]

1) Kimmel Center for Biology and Medicine at the Skirball Institute and Department of Cell Biology, NYU School of Medicine, 540 First Avenue, New York, NY 10016, USA

2) Department of Biology, New York University, New York, NY 10003, USA

3) Corresponding author: Tel: 212-263-1031, Fax: 212-263-7760, Jessica.Treisman@nyulangone.org

4) These two authors contributed equally.

Abstract

The formation of neural circuits requires growing processes to select the correct synaptic partners from a wide array of choices. This recognition depends on interactions between cell surface proteins, but quantitative comparisons of the levels of such proteins have been less considered as a source of synaptic specificity. Here we show that the relative levels of the *Drosophila* CUB-LDL protein Lost and found (Loaf) in the UV-sensitive R7 photoreceptor and its synaptic partners are important for normal R7 axon targeting. Although targeting occurs normally in *loaf* mutant animals, removing *loaf* from photoreceptors or restoring it to the synaptic partner neurons Tm5a/b or Dm9 in a *loaf* mutant causes R7 axons to terminate prematurely. Loaf localizes primarily to intracellular vesicles including endosomes. We suggest that Loaf regulates the trafficking or function of a transmembrane protein, and mismatched levels of this protein on R7 and its synaptic partners prevent stable synapse formation.

Introduction

During nervous system development, growing axons must navigate through a complex environment and select the correct synaptic partners from many potential choices. Recognition of cell surface molecules plays an important role in establishing specific synaptic connections (Yogev and Shen, 2014). In addition to the presence or absence of such molecules, their relative levels can be informative. For instance, gradients of ephrins and their Eph receptors enable retinal axons to form a topographic map in visual areas of the brain because Eph levels determine the sensitivity to ephrins (Triplett and Feldheim, 2012). In the *Drosophila* olfactory system, olfactory receptor neurons preferentially connect to projection neurons that express matching levels of the adhesion molecule Teneurin (Hong et al., 2012). As defects in known synaptic adhesion molecules can lead to autism and other neurodevelopmental disorders (Gilbert and Man, 2017, Van Battum et al., 2015), identifying factors that regulate synaptogenesis is likely to enhance our understanding of the mechanisms of such human diseases.

The *Drosophila* visual system has been a fruitful model for investigations of circuit assembly and synaptic specificity (Plazaola-Sasieta et al., 2017). The two color photoreceptors, R7 and R8, project to distinct layers in the medulla, M6 and M3 respectively. The R7 growth cone first actively targets a temporary layer, and then passively reaches its final layer due to the growth of other neuronal processes (Ting et al., 2005, Ozel et al., 2015). Early stabilization of the R7 and R8 growth cones in different layers depends on differences in their relative levels of the transcription factor Sequoia (Seq); the adhesion molecule N-cadherin (Ncad) is thought to be the relevant target of Seq in these cells (Petrovic and Hummel, 2008, Kulkarni et al., 2016). Both Ncad and the receptor protein tyrosine phosphatase (RPTP) Lar are required to stabilize R7 terminals in the M6 layer. In the absence of either protein they remain in the M3 layer, although defects are observed earlier in development in *Ncad* mutants than in *Lar* mutants (Maurel-Zaffran et al., 2001, Lee et al., 2001, Ting et al., 2005, Ozel et al., 2015, Ozel et al., 2019, Clandinin et al., 2001). Another RPTP, Ptp69D, is partially redundant with Lar, and the depth of R7 axon termination correlates with the total level of RPTP activity (Hofmeyer and Treisman, 2009, Newsome et al., 2000, Hakeda-Suzuki et al., 2017). Stabilization of R7 contacts also requires the presynaptic proteins Liprin-α and Syd-1 that act downstream of Lar (Holbrook et al., 2012, Hofmeyer et al., 2006, Choe et al., 2006, Ozel et al., 2019).

The primary synaptic targets of R7 that are responsible for its function in driving the spectral preference for ultraviolet light are the Dm8 medulla interneurons (Gao et al., 2008, Takemura et al., 2013, Ting et al., 2014, Karuppudurai et al., 2014). These cells fall into two subclasses, yellow (y) and pale (p), and their survival depends on their correct pairing with the appropriate R7 cell subtype, expressing either Rh4 (yR7) or Rh3 (pR7) (Courgeon and Desplan, 2019, Menon et al., 2019). The synapses R7 cells form on Dm8 cells often include the projection neurons Tm5a (for yR7s) or Tm5b (for pR7s) as a second postsynaptic element (Gao et al., 2008, Takemura et al., 2013, Menon et al., 2019). Another interneuron, Dm9, is both pre- and postsynaptic to R7 and R8 and mediates inhibitory interactions between ommatidia (Takemura et al., 2013, Takemura et al., 2015, Heath et al., 2020). It is not known which, if any, of these cell types provide Ncad or RPTP ligands that stabilize filopodia from the R7 growth cone (Hofmeyer and Treisman, 2009, Yonekura et al., 2007, Hakeda-Suzuki et al., 2017, Ozel et al., 2019). Glia are also involved in establishing the pattern of R7 synaptogenesis, as they prevent excessive synapse formation through the adhesion protein Klingon (Klg) and its partner cDIP (Shimozono et al., 2019).

Here we identify a novel CUB-LDL domain protein, Lost and found (Loaf), that acts in photoreceptors to promote the formation of stable R7 contacts in the M6 layer. R7 mistargeting is observed when *loaf* function is lost from photoreceptors, but not in a fully *loaf* mutant animal. Similar defects can be induced in *loaf* mutants by restoring Loaf to neurons that include Tm5a, Tm5b, Dm9 and Dm8, suggesting that R7 targeting is disrupted when R7 has less Loaf than its postsynaptic partners. Loaf does not itself promote cell adhesion and localizes primarily to endosomal membranes. We propose that Loaf controls the trafficking or function of a cell surface molecule that is used to match R7 to the correct postsynaptic neurons.

Results

lost and found is required in photoreceptors for normal R7 axon targeting

A microarray-based screen for genes with enriched expression in the R7 and R8 photoreceptors relative to R1-R6 identified *CG6024*, which encodes an uncharacterized transmembrane protein (Pappu et al., 2011). *CG6024* is also a predicted target of Glass (Naval-Sanchez et al., 2013), a transcription factor required for photoreceptor differentiation and axon guidance (Moses et al., 1989, Selleck and Steller, 1991). To test whether CG6024 had a function in axon targeting by R7 or R8, we expressed RNAi transgenes targeting *CG6024* with two different drivers: *GMR-GAL4* drives expression in all differentiating cell types in the eye (Freeman, 1996), and removing a stop cassette from *Actin>CD2>GAL4* with the eye-specific recombinase $ey^{3.5}$*-FLP* (Bazigou et al., 2007) leads to RNAi expression in the entire eye disc. In both cases, R8 targeting was unaffected, but we observed a loss of R7 terminals from the M6 layer of the medulla (Figure 1A-E); 30-60% of R7 axons were mistargeted to the M3 layer (Figure 1F). We named the gene *lost and found* (*loaf*) based on the failure of R7 axons lacking *loaf* to find the right target layer and on the rescue of this phenotype discussed below. The Loaf protein contains extracellular CUB and LDLa domains and a predicted transmembrane domain (Figure 2A), making it a candidate to directly mediate target recognition by R7.

loaf mutant R7 axons show targeting defects only when *loaf* is present in other cells

Even though we used two independently generated RNAi lines to knock down *loaf*, both of them targeted the same region of the gene (Figure 2A). To confirm that the R7 phenotype was due to loss of *loaf* rather than an off-target effect, we used the CRISPR-Cas9 system to generate deletion alleles that removed the LDLa, transmembrane and cytoplasmic domains of the protein (Figure 2A, I). The sgRNAs were directed against a region of the gene distinct from the RNAi target sequence, and using them to delete the *loaf* gene in the eye by somatic CRISPR reproduced the R7 targeting defect (Figure 2A, B, H). Surprisingly, germline removal of *loaf* resulted in homozygous mutant flies that were viable and showed normal R7 targeting (Figure 2C, D, H), indicating that global loss of *loaf* does not affect this process. In the *loaf* mutant background, expressing *loaf* RNAi

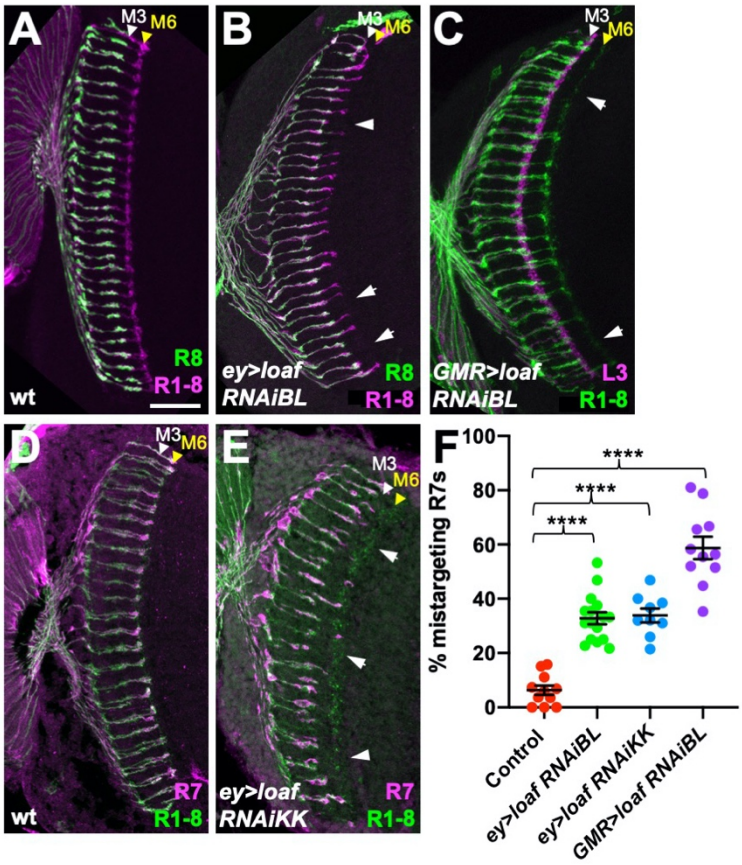

Douthit et al. Figure 1

Figure 1: *loaf* RNAi in photoreceptors causes R7 mistargeting. (A-E) cryostat sections of adult heads stained for Chaoptin (Chp) to label all photoreceptor axons (magenta in A, B, green in C-E), *Rh5-GFP* and *Rh6-GFP* to label R8 (green in A, B), *22E09-LexA* driving *LexAop-myr-tdTomato* to label L3, which projects to the M3 layer (magenta in C) or *panR7-lacZ* to label R7 (magenta in D, E). (A, D) wild type; (B) *ey3.5-FLP, Act>CD2>GAL4; UAS-dcr2; UAS-loaf RNAiBL* (*P{TRiP.JF03040}attP2*); (C) *GMR-GAL4, UAS-dcr2; UAS-loaf RNAiBL*; (E) *ey3.5-FLP, Act>CD2>GAL4; UAS-dcr2; UAS-loaf RNAiKK* (*P{KK112220}VIE-260B*). Arrows show examples of R7 mistargeting. White arrowheads indicate the M3 layer and yellow arrowheads the M6 layer. Scale bar, 20 μm. (F) quantification of the percentage of R7 axons that failed to reach the M6 layer in the same genotypes. n=11 (control, *GMR>RNAiBL*), 16 (*ey>RNAiBL*), or 9 (*ey>RNAiKK*). ****, $p<0.0001$ by unpaired t-test. Error bars show mean ± standard error of the mean (SEM).

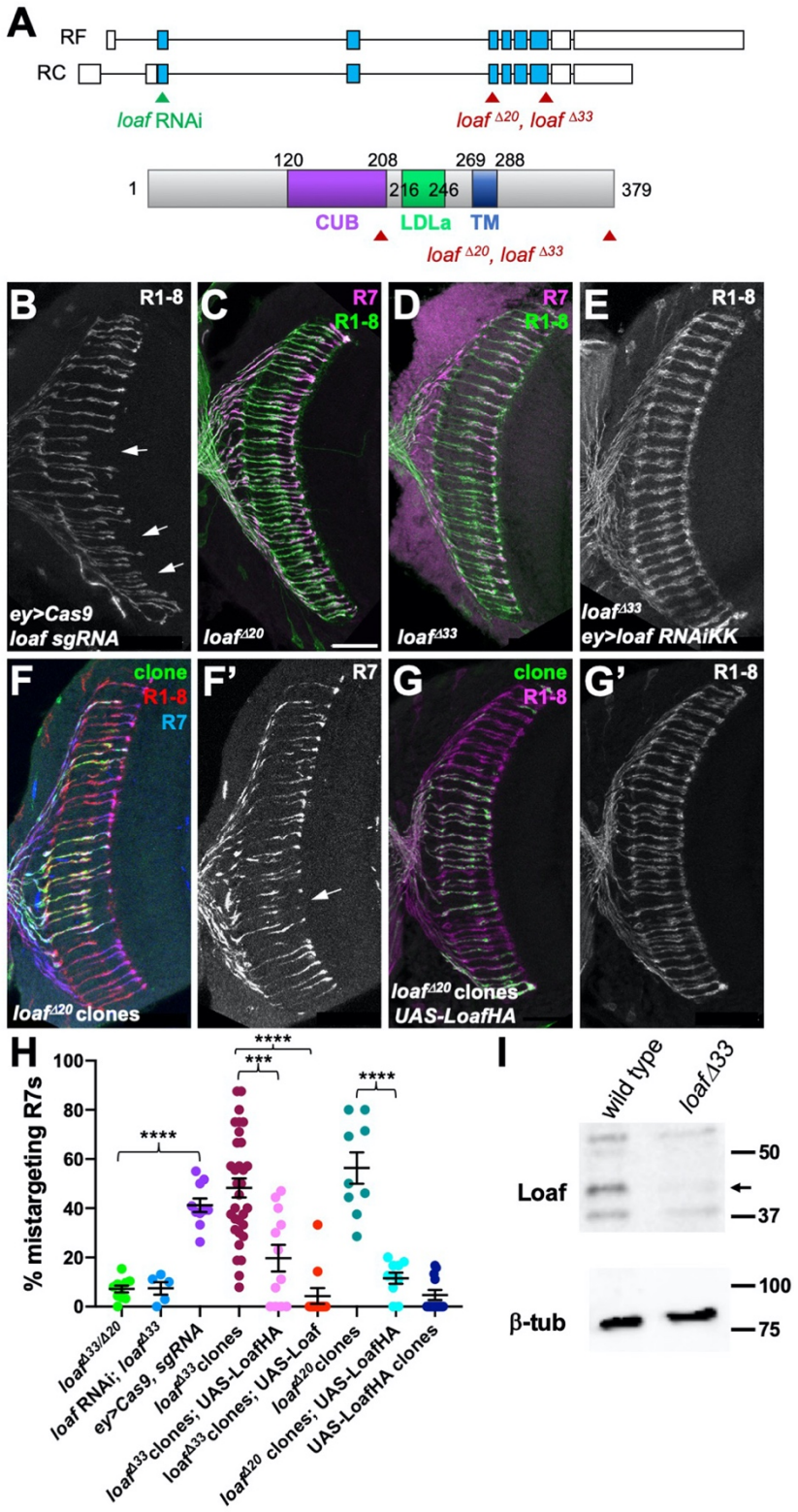

Douthit et al. Figure 2

Figure 2: R7 is only affected by eye-specific loss of *loaf*. (A) diagrams of the *loaf* gene and protein. Coding exons, which are identical for the two isoforms, are shown as blue boxes and non-coding exons as white boxes. The region targeted by both RNAi lines and the positions of the two sgRNAs used to make the *loaf*$^{\Delta 20}$ and *loaf*$^{\Delta 33}$ deletions are indicated. TM, transmembrane domain. (B-G) cryostat sections of adult heads stained for Chp (B, E, G', green in C, D, red in F, magenta in G), *panR7-lacZ* (F', magenta in C, D, blue in F), and GFP (green in F, G). (B) *ey3.5-FLP, Act>CD2>GAL4; loaf sgRNAs; UAS-Cas9P2;* (C) *loaf*$^{\Delta 20}$ homozygote; (D) *loaf*$^{\Delta 33}$ homozygote; (E) *ey3.5-FLP, Act>CD2>GAL4; UAS-dcr2/UAS-loaf RNAiKK; loaf*$^{\Delta 33}$*;* (F) *loaf*$^{\Delta 20}$ clones positively labeled with GFP; (G) *loaf*$^{\Delta 20}$ clones expressing *UAS-LoafHA* with *lGMR-GAL4*, positively labeled with GFP. Scale bar, 20 μm. (H) quantification of the percentage of R7 axons that failed to reach the M6 layer in the indicated genotypes. n=10 (*loaf*$^{\Delta 33}$*/loaf*$^{\Delta 20}$; *ey>Cas9, sgRNA*; *loaf*$^{\Delta 20}$ *clones, UAS-LoafHA*), 5 (*loafRNAi*; *loaf*$^{\Delta 33}$), 32 (*loaf*$^{\Delta 33}$ clones), 12 (*loaf*$^{\Delta 33}$ clones, *UAS-LoafHA*; *UAS-LoafHA* clones), 11 (*loaf*$^{\Delta 33}$ clones, *UAS-Loaf*) or 9 (*loaf*$^{\Delta 20}$ clones). Error bars show mean ± SEM. ***, $p<0.0005$; ****, $p<0.0001$ by unpaired t-test, with Welch's correction when variances are significantly different. *loaf* homozygotes show little R7 mistargeting, but are resistant to the effect of *loaf* RNAi. R7 mistargeting is observed when *loaf* sgRNAs and Cas9 are expressed in the eye, and in clones homozygous for *loaf* alleles. This clonal phenotype is rescued by expressing *UAS-LoafHA* in the mutant cells. (I) Western blot of extracts from wild type and *loaf*$^{\Delta 33}$ larval brains using an antibody to the cytoplasmic domain of Loaf and β-tubulin antibody as a loading control. Loaf protein (arrow) is absent in *loaf*$^{\Delta 33}$ mutants.

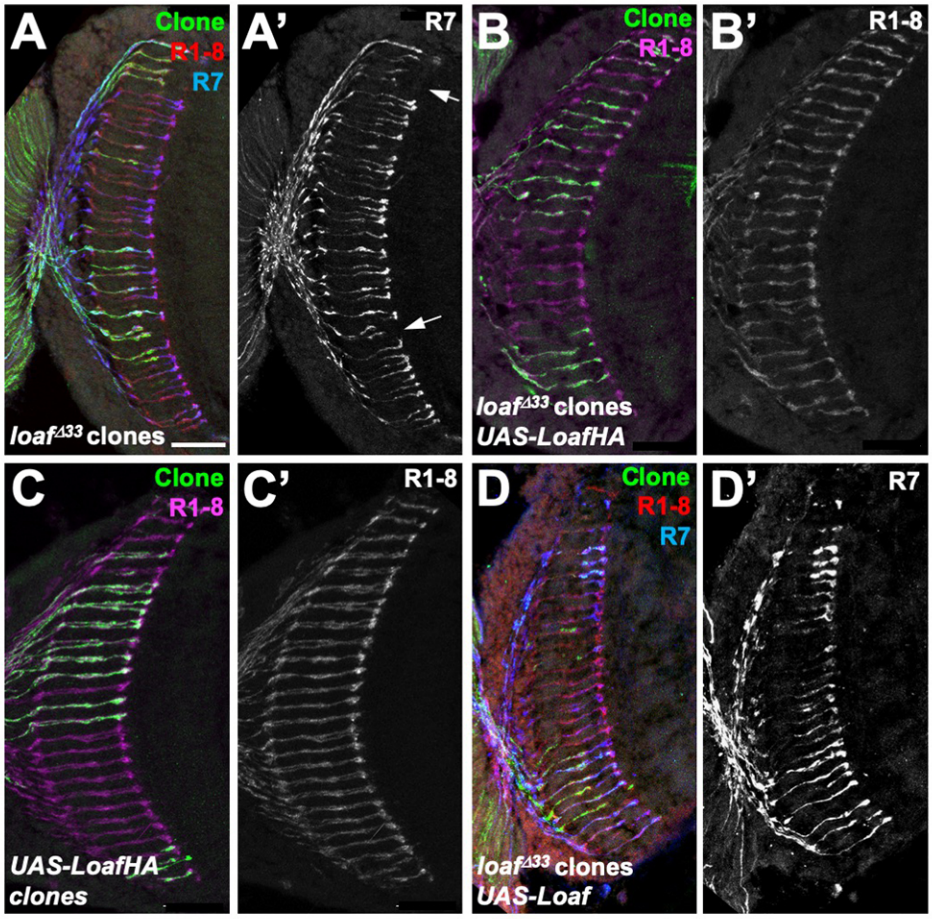

Douthit et al. Figure 2 – figure supplement 1

Figure 2 – figure supplement 1: R7 mistargeting in *loaf* mutant clones is rescued by tagged or untagged Loaf. Cryostat sections of adult heads with clones positively labeled with GFP, stained for Chp (B', C', red in A, D, magenta in B, C), GFP (green) and *panR7-lacZ* (A', D', blue in A, D). (A) *loaf*$^{\Delta 33}$ clones; (B) *loaf*$^{\Delta 33}$ clones expressing *UAS-Loaf-HA* with *lGMR-GAL4*; (C) clones expressing *UAS-Loaf-HA* with *lGMR-GAL4*; (D) *loaf*$^{\Delta 33}$ clones expressing *UAS-Loaf* with *lGMR-GAL4*. Scale bar, 20 μm.

had no effect (Figure 2E, H), confirming that the RNAi phenotype was due to its effect on *loaf* rather than another gene. Together, these results indicate that the phenotype caused by removing *loaf* from photoreceptors is dependent on the presence of *loaf* elsewhere in the animal. R7 targeting may depend on the amount of Loaf in R7 relative to other cells rather than its absolute quantity.

To test this hypothesis, we generated clones of cells in the eye that were homozygous for *loaf* deletion alleles in an otherwise heterozygous background. As predicted, these showed mistargeting of R7 axons to the M3 layer (Figure 2F, H, Figure 2 – figure supplement 1A). The mistargeting was significantly rescued by expressing either HA-tagged or untagged Loaf within the mutant clones (Figure 2G, H, Figure 2 – figure supplement 1B-D), confirming that it is due to loss of *loaf* from photoreceptors. These results could be explained if correct targeting requires R7 to compare its level of Loaf to that of another cell type. A reduction of Loaf in R7 relative to this cell type would cause mistargeting. When Loaf is absent from all cells, redundant mechanisms may be sufficient to maintain R7 terminals in the correct layer.

Matching Loaf levels in R7 and its major synaptic target Dm8 are not required for targeting

The medulla interneuron Dm8, which mediates the preference for ultraviolet over visible light, was reported to be the major postsynaptic target of R7 (Gao et al., 2008, Takemura et al., 2013, Ting et al., 2014). We therefore considered the hypothesis that R7 and its postsynaptic partner Dm8 must have matching Loaf levels to form a stable synapse (Figure 3F). We first determined the effect of removing *loaf* function from Dm8. Expressing *loaf* RNAi or Cas9 and *loaf* sgRNAs in neurons that include Dm8 cells with *DIP-γ-GAL4* or *traffic jam* (*tj*)-*GAL4* (Carrillo et al., 2015, Courgeon and Desplan, 2019) did not cause any R7 targeting phenotype (Figure 3 – figure supplement 1A, B). As it was difficult to assess the reduction in Loaf levels caused by these manipulations, we generated *loaf* mutant clones in the brain and labeled the mutant Dm8 cells with *ortc2b-GAL4* (Ting et al., 2014). R7 axons that contacted the dendrites of mutant Dm8 cells correctly reached the M6 layer, and there was no obvious defect in the position or morphology of the mutant dendrites (Figure 3A, B).

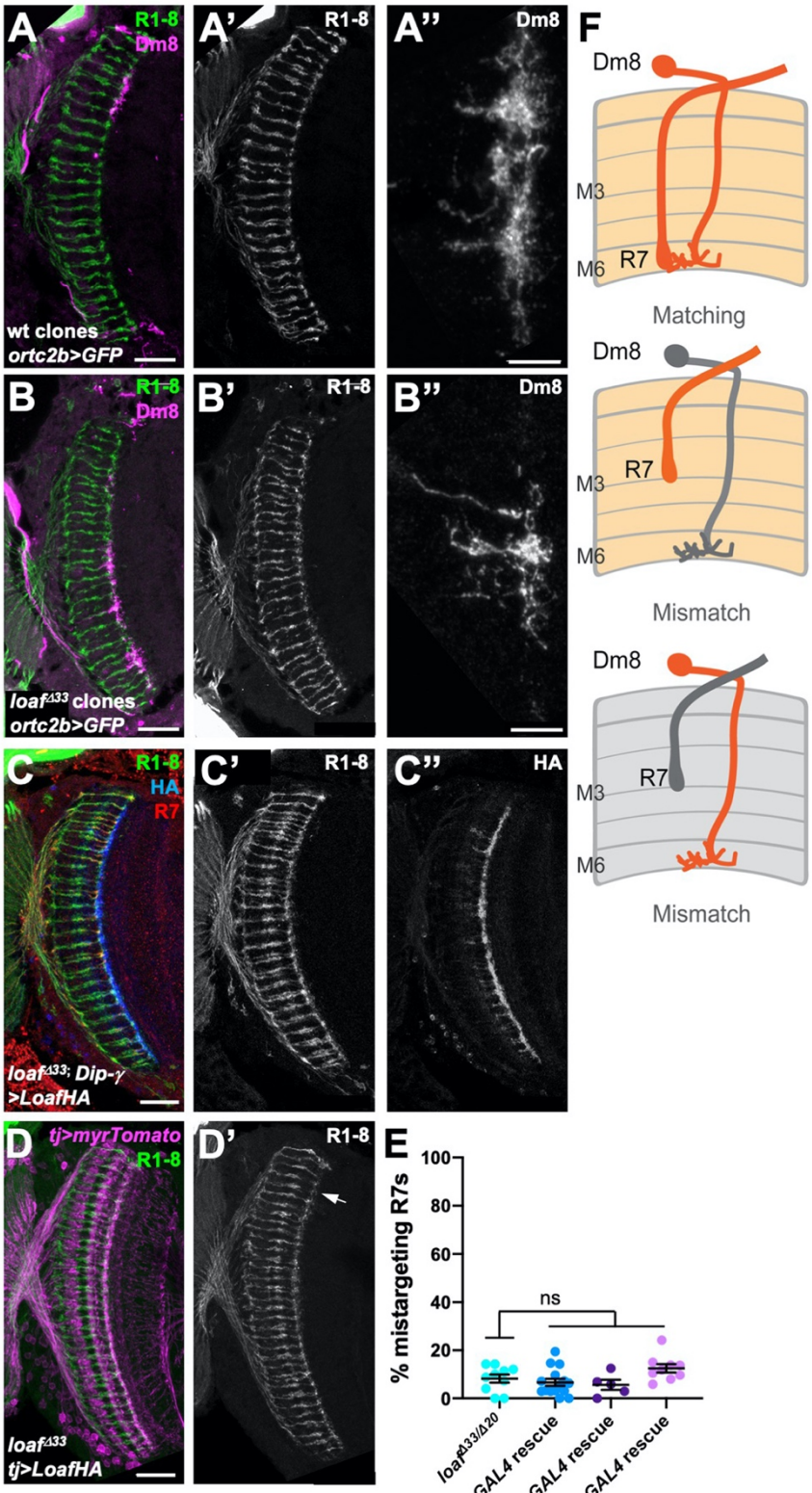

Douthit et al. Figure 3

Figure 3: Changing the level of Loaf in Dm8 does not affect R7 targeting. (A-D) cryostat sections of adult heads stained for Chp (A'-D', green in A-D), GFP (A'', B'', magenta in A, B), *panR7-lacZ* (red in C), HA (C'', blue in C) or myrTomato (magenta in D). (A) wild type clones in which Dm8 is labeled with *ortc2b-GAL4, UAS-CD8GFP*; (B) *loaf*$^{\Delta 33}$ clones in which Dm8 is labeled with *ortc2b-GAL4, UAS-CD8GFP*. (A'' and B'' show enlargements of labeled Dm8 dendrites. *loaf* mutant Dm8 dendrites and the R7 axons that target them have the normal position and morphology. (C) *UAS-LoafHA; DIP-γ-GAL4, loaf*$^{\Delta 33}$*/loaf*$^{\Delta 33}$; (D) *tj-GAL4/UAS-LoafHA; loaf*$^{\Delta 33}$*/loaf*$^{\Delta 33}$. Scale bars, 20 μm (A-D), 5 μm (A'', B''). (E) quantification of the percentage of R7 axons that failed to reach the M6 layer in the indicated genotypes. n=10 (*loaf*$^{\Delta 33}$*/loaf*$^{\Delta 20}$*; DIP-γ-GAL4* rescue*; tj-GAL4* rescue), or 5 (*drf-GAL4* rescue). Error bars show mean ± SEM. ns, not significant by unpaired t-test. Restoring Loaf to Dm8 precursors in a *loaf* mutant does not cause R7 mistargeting. (F) diagrams explaining the matching model. R7 and Dm8 express matching levels of Loaf (orange), which is also present in other cells in the brain. Removing *loaf* from Dm8 (gray) or restoring Loaf to Dm8 in a *loaf* mutant (gray in R7 and brain) would cause a mismatch.

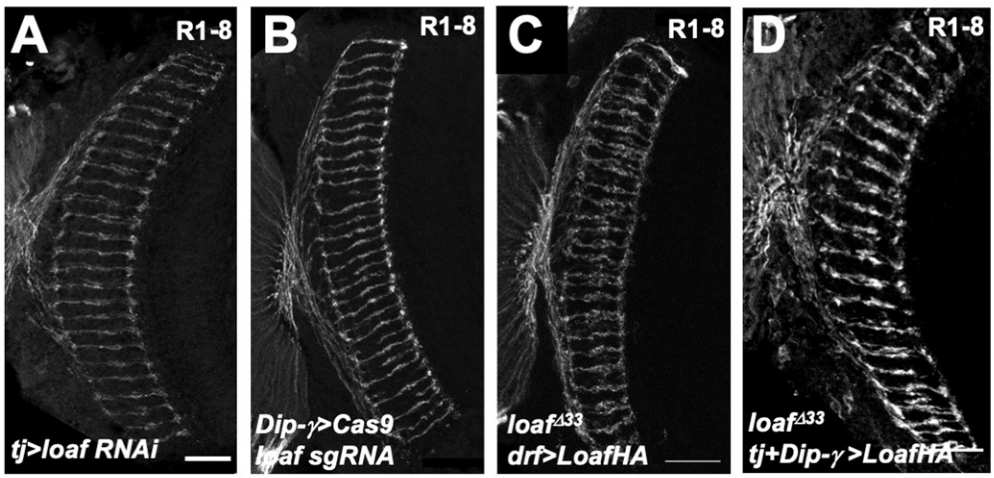

Douthit et al. Figure 3 – figure supplement 1

Figure 3 – figure supplement 1: Changing Loaf levels in Dm8 has no effect. Cryostat sections of adult heads stained for Chp. (A) *tj-GAL4*; *loaf RNAiBL*; (B) *loaf sgRNAs*; *DIP-γ-GAL4/UAS-Cas9P2*; (C) *UAS-LoafHA*; *drf-GAL4*, $loaf^{\Delta 33}$/ $loaf^{\Delta 33}$; (D) *tj-GAL4*/*UAS-LoafHA*; *DIP-γ-GAL4*, $loaf^{\Delta 33}$/$loaf^{\Delta 33}$. Scale bar, 20 μm.

Another prediction of the matching hypothesis is that restoring Loaf to Dm8 cells in a *loaf* mutant background would result in a mismatch between R7 and Dm8, similar to removing *loaf* from R7 in a wild-type background (Figure 3F). We tested this by expressing UAS-Loaf-HA in *loaf* mutant flies with the Dm8 drivers *DIP-γ-GAL4*, *tj-GAL4* and *drifter* (*drf*)-*GAL4* (Carrillo et al., 2015, Courgeon and Desplan, 2019, Hasegawa et al., 2011), as well as a combination of *tj-GAL4* and *DIP-γ-GAL4*. Again, we did not observe significant levels of R7 mistargeting (Figure 3C-E, Figure 3 – figure supplement 1C, D), arguing against a requirement for matching Loaf levels in R7 and Dm8.

R7 compares its Loaf levels with cholinergic and glutamatergic neurons

An alternative hypothesis that might explain our results is that R7 uses Loaf to compete with another Loaf-expressing cell type for access to the M6 layer (Figure 4D). In this case, restoring Loaf to that cell type in a *loaf* mutant should put R7 at a disadvantage and result in its mistargeting. To identify potential competitors, we used several methods to examine the location of Loaf expression in the brain. RNA-Seq analysis of sorted cell types in the adult brain revealed widespread expression of *loaf*, although at varying levels (Konstantinides et al., 2018, Davis et al., 2020). However, Loaf translation in photoreceptors reaches its maximum at mid-pupal stages, when R7 axons are targeting the M6 layer (Zhang et al., 2016, Ting et al., 2005), so adult expression levels in other cells might not be reflective of this developmental stage. We examined the expression at pupal stages of a GFP protein trap insertion in *loaf*. It also appeared to be expressed in many cells in the medulla, and was more highly localized to cell bodies than to neuronal processes (Figure 4A). Finally, we generated an antibody to the cytoplasmic domain of Loaf (Figure 2I). Pupal brains showed strong staining in numerous cell bodies and weaker staining throughout the neuropil, both of which were absent in *loaf* mutants (Figure 4B, C).

Because these experiments did not identify a specific cell type that would be most likely to compete with R7 using Loaf, we tested whether R7 mistargeting could be induced by restoring Loaf to broad categories of cells in a *loaf* mutant background. We observed no phenotype when Loaf was expressed in glia with *repo-Gal4*, or in neuronal populations that expressed *homothorax* (*hth*)-*GAL4*, *brain-specific homeobox* (*bsh*)-*GAL4*, or *Visual system homeobox* (*Vsx)-GAL4* (Li et al., 2013, Erclik et al., 2017, Hasegawa et al., 2011) (Figure 4G). However, we did observe a significant

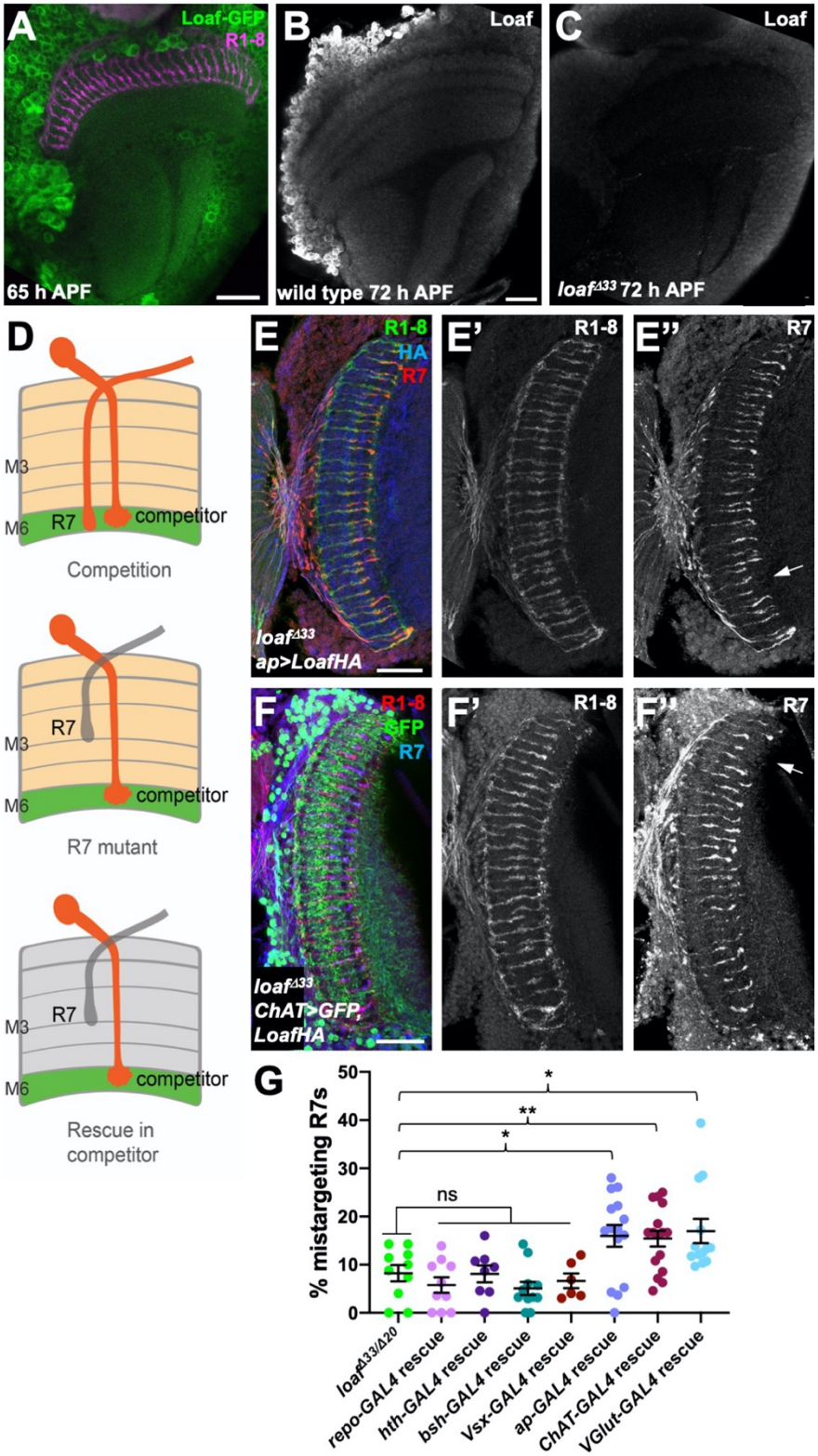

Douthit et al. Figure 4

Figure 4: R7 compares its level of Loaf with cholinergic and glutamatergic neurons. (A-C) pupal brains at 65 h after puparium formation (APF) (A) or 72 h APF (B, C), stained for GFP (green in A), Chp (magenta in A) or Loaf (B, C). (A) Loaf protein trap *Mi{PT-GFSTF.1}CG6024*$^{MI00316\text{-}GFSTF.1}$; (B) wild type; (C) *loaf*$^{\Delta 33}$. Loaf antibody and the protein trap both label many cell bodies in the medulla and show weaker staining in the neuropil. Antibody staining is lost in the *loaf* mutant. (D) diagram explaining the competition model. R7 and a competitor neuron use Loaf (orange) to compete for access to the M6 layer (green). Removal of *loaf* from R7 (gray) or expression of Loaf in the competitor neuron in a *loaf* mutant background (R7 and brain gray) would cause R7 to lose the competition and terminate in the M3 layer. (E, F) cryostat sections of adult heads stained for Chp (E', F', green in E, red in F), *panR7-lacZ* (E'', F'', red in E, blue in F), HA (blue in E) or GFP (green in F). (E) *ap-GAL4/UAS-LoafHA; loaf*$^{\Delta 33}$; (F) *ChAT-GAL4, UAS-CD8GFP/UAS-LoafHA; loaf*$^{\Delta 33}$. Scale bars, 20 μm. (G) quantification of the percentage of R7 axons that failed to reach the M6 layer in the indicated genotypes. n=10 (*loaf*$^{\Delta 33}$*/loaf*$^{\Delta 20}$*; repo-GAL4* rescue) 8 (*hth-GAL4* rescue), 11 (*bsh-GAL4* rescue), 6 (*Vsx-GAL4* rescue), 15 (*ap-GAL4* rescue), 16 (*ChAT-GAL4* rescue) or 13 (*vGlut-GAL4* rescue). Error bars show mean ± SEM. *, $p<0.05$; **, $p<0.01$; ns, not significant by unpaired t-test. Restoring Loaf to cholinergic or glutamatergic neurons or expressing it in the precursors of cholinergic neurons with *ap-GAL4* in a *loaf* mutant causes R7 mistargeting.

level of R7 mistargeting when Loaf was expressed in neurons that expressed *apterous* (*ap*)-*GAL4* (Li et al., 2013) or in cholinergic neurons with *Choline acetyltransferase* (*ChAT*)-*GAL4* (Figure 4E-G). *ap* is expressed in the majority of cholinergic neurons in the medulla (Konstantinides et al., 2018), supporting a role for cells in this population. R7 targeting defects also occurred when Loaf was restored to glutamatergic neurons in a *loaf* mutant background with *Vesicular glutamate transporter* (*VGlut*)-*GAL4* (Figure 4G), indicating that more than one type of neuron is involved in the comparison of Loaf levels.

R7 may match its Loaf levels with multiple synaptic target cells

The populations of cholinergic and glutamatergic neurons include other synaptic targets of Loaf, making the matching hypothesis still a possibility. To test the involvement of the cholinergic neurons Tm5a and Tm5b (Davis et al., 2020), which are postsynaptic to R7 (Gao et al., 2008, Menon et al., 2019), we used *GMR9D03-GAL4*, which is expressed in a subset of these cells (Figure 5 – figure supplement 1A, B). Expressing Loaf with this driver in a *loaf* mutant background again produced significant R7 mistargeting (Figure 5A, H), consistent with the hypothesis that R7 matches its Loaf levels to Tm5a/b. Although *GMR9D03-GAL4* is also expressed in some lamina neurons, restoring Loaf only in lamina neurons with *GH146-GAL4* (Schwabe et al., 2014) did not affect R7 (Figure 5H). However, *loaf* mutant Tm5a/b cells did not have obvious morphological defects or cause R7 mistargeting (Figure 5D, E).

Among glutamatergic neurons, both Dm8 and Dm9 are synaptic partners of R7. Dm9 is a multicolumnar neuron that tracks R7 axons closely and mediates inhibition between neighboring ommatidia (Nern et al., 2015, Heath et al., 2020). The transcription factors Vestigial (Vg) and Defective proventriculus (Dve) are strongly enriched in Dm9 cells (Davis et al., 2020), and *dve-GAL4* drives expression in Dm9 (Figure 5 – figure supplement 1C), although *vg-GAL4* expression was not detectable in the adult brain. When used to express Loaf in a *loaf* mutant, neither driver alone significantly affected R7 targeting, but the combination had a significant effect (Figure 5B, H), making Dm9 a candidate to match Loaf levels with R7. Again, *loaf* mutant Dm9 cells and their presynaptic R7 axons appeared normal (Figure 5F, G). Finally, we tested whether Dm8 might make a contribution in combination with other synaptic target cells by restoring Loaf with both *ap-GAL4* and *tj-GAL4*. This produced significantly more R7 mistargeting than *ap-GAL4* alone (Figure 5C, H),

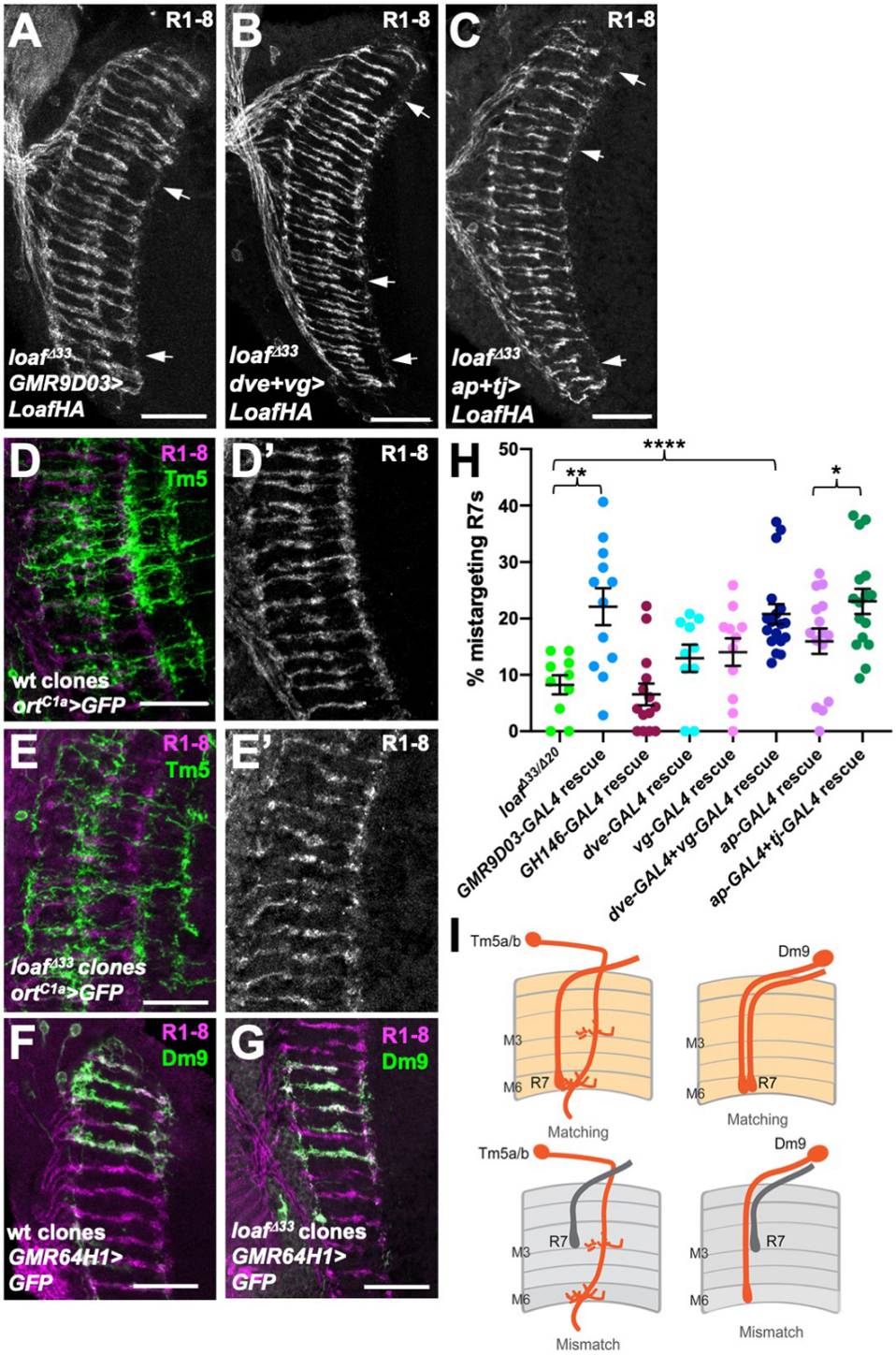

Douthit et al. Figure 5

Figure 5: Restoring Loaf to synaptic partners of R7 in a *loaf* mutant causes mistargeting. (A-C) cryostat sections of adult heads stained for Chp. (A) *UAS-LoafHA*; *GMR9D03-GAL4*, $loaf^{\Delta 33}/loaf^{\Delta 33}$; (B) *dve-GAL4*, *vg-GAL4*/*UAS-LoafHA*; $loaf^{\Delta 33}$; (C) *ap-GAL4, tj-GAL4*/*UAS-LoafHA*; $loaf^{\Delta 33}$. Expressing Loaf in populations of neurons that form synapses with R7 in a *loaf* mutant background causes R7 mistargeting. (D-G) cryostat sections of adult heads in which clones generated with *hs-FLP* are labeled in green with UAS-CD8-GFP and R1-8 are stained with anti-Chp (D', E', magenta in D-G). (D) wild type and (E) $loaf^{\Delta 33}$ mutant clones in which Tm5a/b/c and Tm20 are labeled with ort^{C1a}*-GAL4*. (F) wild type and (G) $loaf^{\Delta 33}$ mutant clones in which Dm9 cells are labeled with *GMR64H1-GAL4*. The morphologies of wild type and *loaf* mutant cells appear similar. (H) quantification of the percentage of R7 axons that failed to reach the M6 layer in the indicated genotypes. n=10 ($loaf^{\Delta 33}/loaf^{\Delta 20}$; *dve-GAL4* rescue), 12 (*GMR9D03-GAL4* rescue), 14 (*GH146-GAL4* rescue), 11 (*vg-GAL4* rescue), 18 (*dve-GAL4* + *vg-GAL4* rescue), 15 (*ap-GAL4* rescue), 16 (*ap-GAL4* + *tj-GAL4* rescue). Error bars show mean ± SEM. *, $p<0.05$; **, $p<0.01$; ****, $p<0.0001$ by unpaired t-test. (I) model showing that mismatched Loaf levels between R7 and Dm9 or R7 and Tm5a/b when *loaf* is restored to these cells in a *loaf* mutant could cause R7 mistargeting. Scale bars, 20 μm.

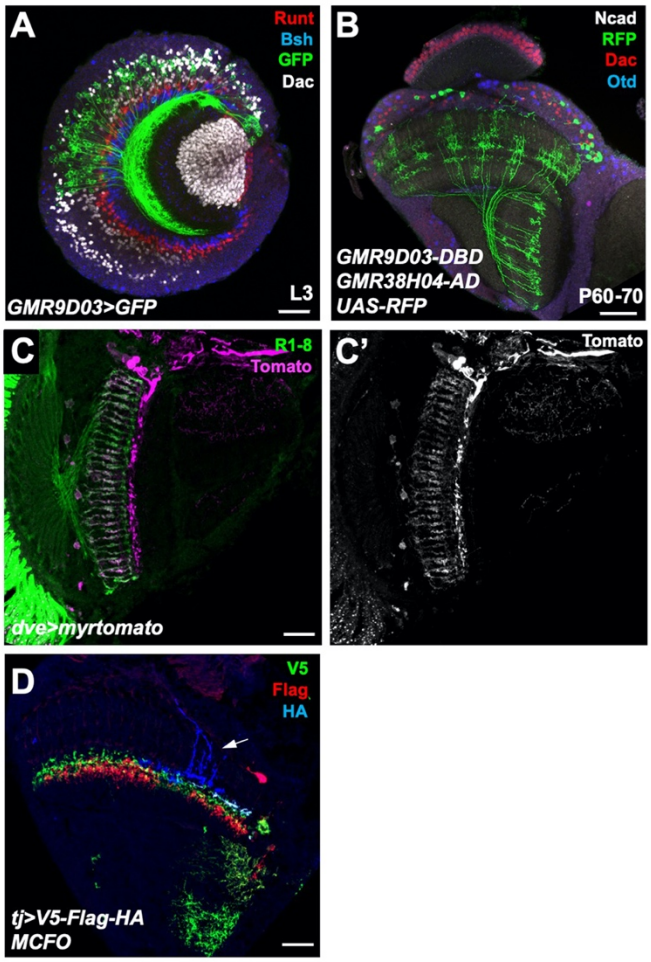

Douthit et al. Figure 5 – figure supplement 1

Figure 5 – figure supplement 1: GAL4 drivers for Tm5a/b and Dm9. (A) a third instar larval brain expressing *UAS-CD8-GFP* with *GMR9D03-GAL4*, stained for GFP (green), Dac (white), Runt (red) and Bsh (blue). *GMR9D03-GAL4*-expressing cell bodies do not express Bsh, Runt or Dac, consistent with Tm5a/b identity, and are restricted to the dorsal half of the medulla. (B) pupal brain at 60-70 h APF expressing *UAS-RFP* with the split-GAL4 lines *GMR9D03-DBD* and *GMR38H04-AD*, stained for RFP (green), Dac (red), Otd (blue) and Ncad (white). Cells with the morphology and projection pattern of Tm5a/b that are negative for Dac and Otd are labeled with RFP, showing that the *GMR9D03* enhancer is expressed in a subset of these cells. (C) cryostat section of adult head expressing *UAS-myr-tdTomato* with *dve*^{NP3428}*-GAL4*, stained for Tomato (C', magenta in C) and Chp (green). *dve*^{NP3428}*-GAL4* labels cells with the morphology and projection pattern of Dm9. (D) *tj-GAL4* expressing cells labeled with V5 (green), FLAG (red) and HA (blue) using the MultiColor FlpOut (MCFO) system. The cell labeled in blue (arrow) resembles a Dm11 cell.

suggesting that Dm8 or another *tj-GAL4* expressing neuron such as Dm11 (Courgeon and Desplan, 2019), which also projects to the M6 layer (Nern et al., 2015) (Figure 5 -figure supplement 1D), may contribute to matching the levels of Loaf to its postsynaptic targets. However, Tm5a/b and Dm9 appear to play a more significant role (Figure 5I).

Loaf may act indirectly through a cell-surface molecule

To determine whether Loaf could function as a homophilic cell adhesion molecule, we transfected HA-tagged Loaf into S2 cells and conducted cell aggregation assays (Ting et al., 2005, Astigarraga et al., 2018). We did not observe significant aggregation of the transfected cells, although the positive control Sidekick (Sdk) (Astigarraga et al., 2018) induced aggregation under the same conditions (Figure 6A, B, Figure 6 – figure supplement 1A). Unlike Sdk, neither tagged nor untagged Loaf showed strong localization to the plasma membrane; most Loaf was present in punctate structures inside the cells (Figure 6C-E). These structures showed partial colocalization with Hepatocyte growth factor-regulated tyrosine kinase substrate (Hrs) and Rab7 (Figure 6D, E), two markers of late endosomes, but did not colocalize with the recycling endosome marker Rab11-GFP (Figure 6 – figure supplement 1B). Loaf-HA also partially colocalized with Rab7 and Hrs, but not with the lysosomal markers ADP-ribosylation factor-like 8 (Arl8) or Vacuolar H^+-ATPase 55kD subunit (Vha55), when expressed in the retina in vivo (Figure 6F, G, I), and untagged Loaf again showed a similar localization (Figure 6 – figure supplement 1C). When expressed in clones of cells mutant for the ESCRT complex component *Tumor susceptibility gene 101* (*TSG101*), in which endocytosed proteins such as Notch accumulate in late endosomes (Moberg et al., 2005), Loaf-HA colocalized with Notch (Figure 6 – figure supplement 1D), confirming its presence in the endocytic pathway. GFP-tagged endogenous Loaf also appeared to localize to the cytoplasm of photoreceptors, although unlike overexpressed Loaf, it was primarily found close to the plasma membrane rather than in late endosomes (Figure 6H). These results suggest that Loaf is not itself a cell surface adhesion molecule, but could regulate the trafficking or cell surface localization of another protein that regulates cell adhesion or synapse formation.

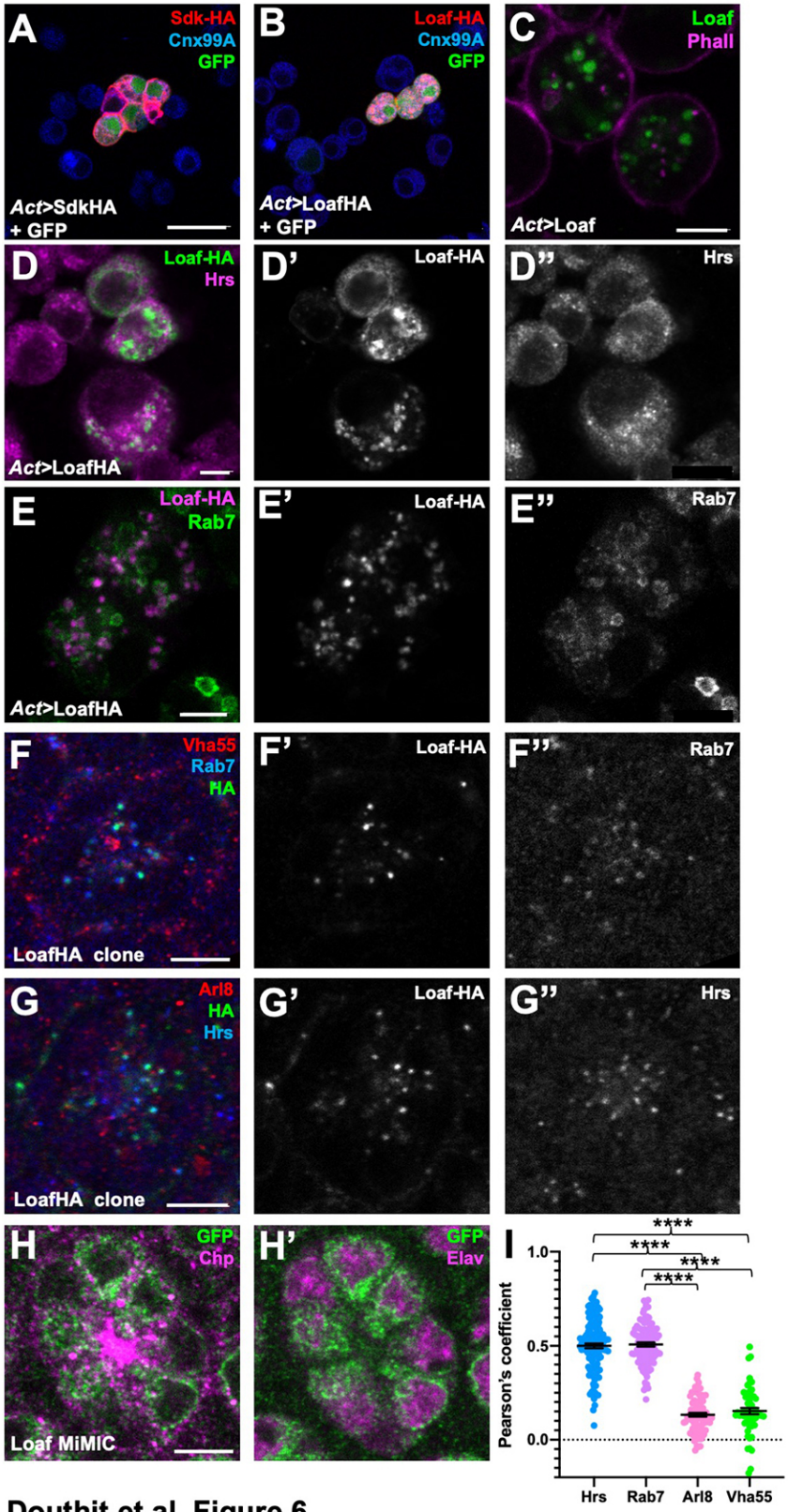

Douthit et al. Figure 6

Figure 6: Loaf localizes to endosomes. (A, B) S2 cells transfected with *Act-GAL4*, *UAS-GFP* and *UAS-SdkHA* (A) or *UAS-LoafHA* (B) and allowed to aggregate, stained for GFP (green), HA (red) and Cnx99A (blue). Sdk localizes to cell contacts and induces aggregation, but Loaf does not. (C) S2 cells transfected with *Act-GAL4* and *UAS-Loaf*, stained with anti-Loaf (green) and Phalloidin (magenta). (D, E) S2 cells transfected with *Act-GAL4* and *UAS-LoafHA*, stained for HA (D', E', green in D, magenta in E), Hrs (D'', magenta in D), or Rab7 (E'', green in E). Loaf localizes to intracellular vesicles that show some colocalization with Hrs and Rab7. (F, G) ommatidia from 42 h APF pupal retinas in clones expressing UAS-LoafHA, stained for HA (F', G', green in F, G) Rab7 (F'', blue in F), Vha55 (red in F), Hrs (G'', blue in G) and Arl8 (red in G). Loaf colocalizes with the endosomal markers Rab7 and Hrs, but not the lysosomal markers Vha55 and Arl8, in photoreceptors in vivo. (H) Ommatidium from a Loaf protein trap *Mi{PT-GFSTF.1}CG6024*$^{MI00316\text{-}GFSTF.1}$ retina, stained for GFP (green), Chp (magenta in H) and Elav (magenta in H'). Endogenous Loaf-GFP is present just inside the plasma membrane marked by Chp and in the cytoplasm close to the rhabdomere. (I) quantification of the colocalization of Loaf-HA with Hrs, Rab7, Arl8 and Vha55 in 42 h APF retinas by Pearson's correlation. n=131 ommatidia from 19 retinas (Hrs), 100 ommatidia from 19 retinas (Rab7), 85 ommatidia from 16 retinas (Arl8) or 59 ommatidia from 11 retinas (Vha55). Error bars show mean ± SEM. ****, $p<0.0001$. Scale bars, 20 μm (A) or 5 μm (C-H).

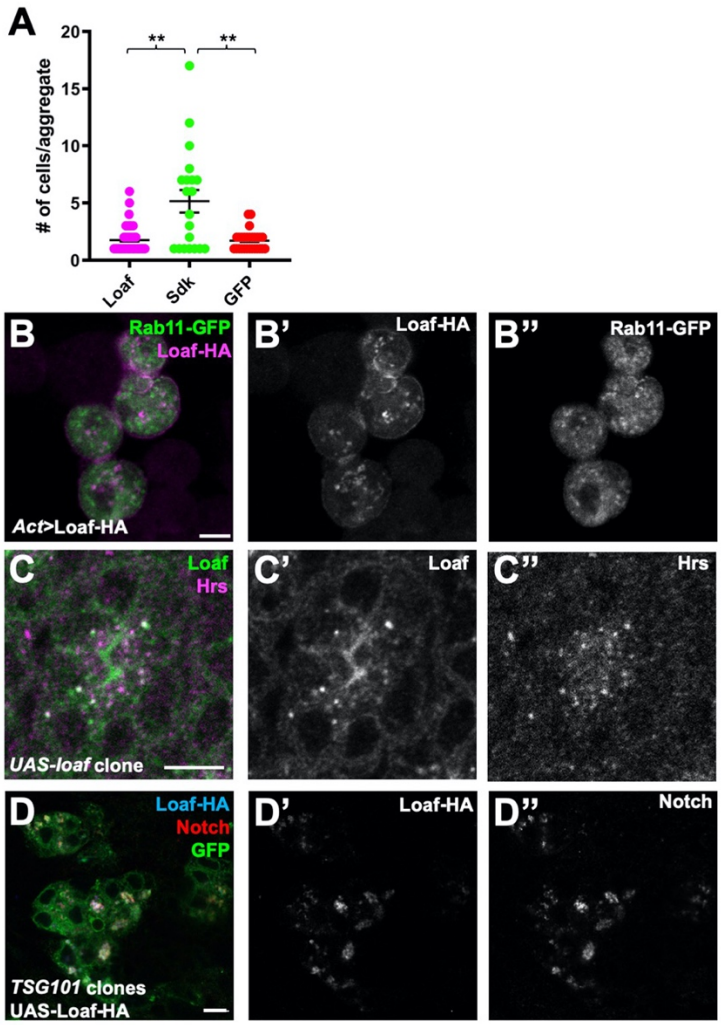

Douthit et al. Figure 6 – figure supplement 1

Figure 6 – figure supplement 1: Loaf localizes to endosomes and does not mediate cell aggregation. (A) quantification of the number of cells per aggregate for S2 cells transfected with *Act-GAL4* and *UAS-LoafHA*, *UAS-SdkHA*, or *UAS-GFP*. n=63 (Loaf), 20 (Sdk) or 27 (GFP). **, p<0.01 by unpaired t-test with Welch's correction. (B) S2 cells transfected with *Act-GAL4*, *UAS-Loaf-HA* and *UAS-Rab11-GFP*, stained for HA (B', magenta in B) and GFP (B'', green in B). Loaf does not colocalize with Rab11. (C) ommatidium from a 42 h APF retina from a clone expressing *UAS-Loaf*, stained for Loaf (C', green in C) and Hrs (C'', magenta in C). Untagged Loaf colocalizes with Hrs in vivo. (D) ommatidium from a 42 h APF retina from a *TSG101* clone in which *UAS-LoafHA* was expressed with *lGMR-GAl4*, positively labeled with GFP and stained for GFP (green), HA (D', blue in D) and Notch (D'', red in D). Loss of *TSG101* causes accumulation of enlarged endosomes in which Loaf colocalizes with internalized Notch. Scale bars, 5 μm.

Loaf affects the activity of Lrp4

We next searched for candidate proteins that might be regulated by Loaf. One possibility we considered was Lar, an RPTP that is required for normal R7 targeting (Maurel-Zaffran et al., 2001, Hofmeyer and Treisman, 2009, Clandinin et al., 2001). Although *Lar* mutants have a strong mistargeting phenotype, *Lar* acts in R7 and not the target region (Clandinin et al., 2001, Maurel-Zaffran et al., 2001), so its ligand, which remains unknown, would also have to be regulated by Loaf to fit the matching hypothesis. We found that *loaf* was not required for HA-tagged Lar to be transported into photoreceptor axons (Figure 7 – figure supplement 1A-B). Overexpression of Lar in photoreceptors, either alone or together with Loaf, did not cause any significant defects (Figure 7A, B, D). Interestingly, overexpression of Lar in *loaf* mutant photoreceptors could rescue R7 targeting (Figure 7C, D), indicating that Lar can compensate for the lack of *loaf* and is thus unlikely to be its primary effector.

We also investigated LDL receptor related protein 4 (Lrp4), based on its role as a presynaptic organizer in the olfactory system (Mosca et al., 2017), its postsynaptic signaling function at the vertebrate neuromuscular junction (Yumoto et al., 2012), and the requirement for chaperones to promote the trafficking of other LDL family members (Wagner et al., 2013, Culi et al., 2004). We found evidence that the level of Lrp4 can affect R7 targeting and that its activity is regulated by Loaf. Overexpressing Lrp4 in photoreceptors causes R7 axons to contact each other or hyperfasciculate either in the M3 or M6 layers of the medulla (Figure 7E, H). These defects are more severe, and include overshooting of the M6 layer by some R7 axons, when Lrp4 is coexpressed with Loaf (Figure 7F, H), and are less severe when Lrp4 is expressed in *loaf* mutant photoreceptors (Figure 7G, H). Lrp4 overexpression also results in abnormal numbers and arrangements of cone and pigment cells in the retina (Figure 7 – figure supplement 1C). Again, these defects are more severe when Lrp4 is coexpressed with Loaf, and largely absent when Lrp4 is expressed in *loaf* mutant cells (Figure 7 – figure supplement 1D, E). Although Lrp4-HA had a more granular appearance in *loaf* mutant than in wild type photoreceptor cell bodies (Figure 7 – figure supplement 1F, H), it was still transported into their axons (Figure 7 - figure supplement 1G, I), and its level of expression appeared unaffected (Figure 7 - figure supplement 1J). Lrp4 is unlikely to fully explain the effects of *loaf* on R7 targeting, as R7 axons projected normally in *Lrp4* mutant clones (Figure 7 - figure supplement 1K), and expressing *loaf* RNAi in photoreceptors resulted in R7

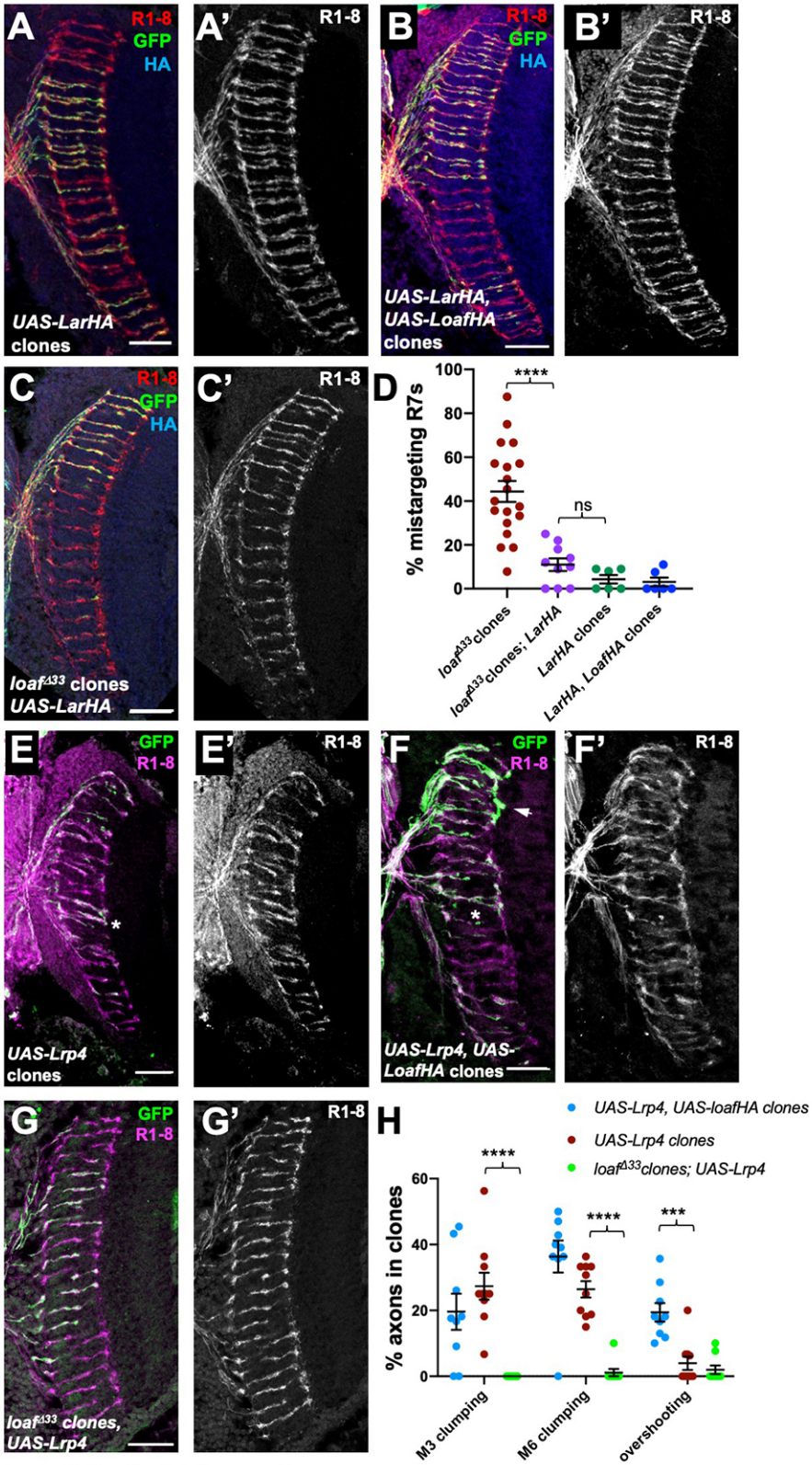

Douthit et al. Figure 7

Figure 7: *loaf* genetically interacts with *Lrp4*. (A-C) cryostat sections of adult heads with clones positively labeled with GFP, stained for Chp (A', B', C', red in A-C), GFP (green) and HA (blue). (A) clones expressing *UAS-Lar-HA* with *lGMR-GAL4*. (B) clones expressing *UAS-Lar-HA* and *UAS-Loaf-HA* with *lGMR-GAL4*. (C) $loaf^{\Delta 33}$ clones in which *UAS-Lar-HA* is expressed with *lGMR-GAL4*. (D) quantification of the percentage of R7 axons that failed to reach the M6 layer in the indicated genotypes. Expressing *Lar* rescues mistargeting in *loaf* mutant clones. n=19 ($loaf^{\Delta 33}$ clones), 10 ($loaf^{\Delta 33}$ clones; *LarHA*), or 6 (*LarHA* clones; *LarHA*, *LoafHA* clones). Error bars show mean ± SEM. ****, p<0.0001; ns, not significant by unpaired t-test with Welch's correction. (E-G) cryostat sections of adult heads with clones positively labeled with GFP, stained for Chp (E', F', G', magenta in E-G) and GFP (green). (E) clones expressing *UAS-Lrp4* with *lGMR-GAL4*. (F) clones expressing *UAS-Lrp4* and *UAS-Loaf-HA* with *lGMR-GAL4*. (C) $loaf^{\Delta 33}$ clones in which *UAS-Lrp4* is expressed with *lGMR-GAL4*. (H) quantification of the percentage of labeled R7s of each genotype that show R7 axons clumping together in the M3 (asterisk in F) or M6 (asterisk in E) layers or overshooting the M6 layer (arrow in F). n=9 heads (*UAS-Lrp4*, *UASLoafHA*; $loaf^{\Delta 33}$ clones, *UAS-Lrp4*) or 10 (*UAS-Lrp4*). Error bars show mean ± SEM. ***, p<0.001; ****, p<0.0001 by multiple t-tests with two-stage linear step-up procedure. Scale bars, 20 μm.

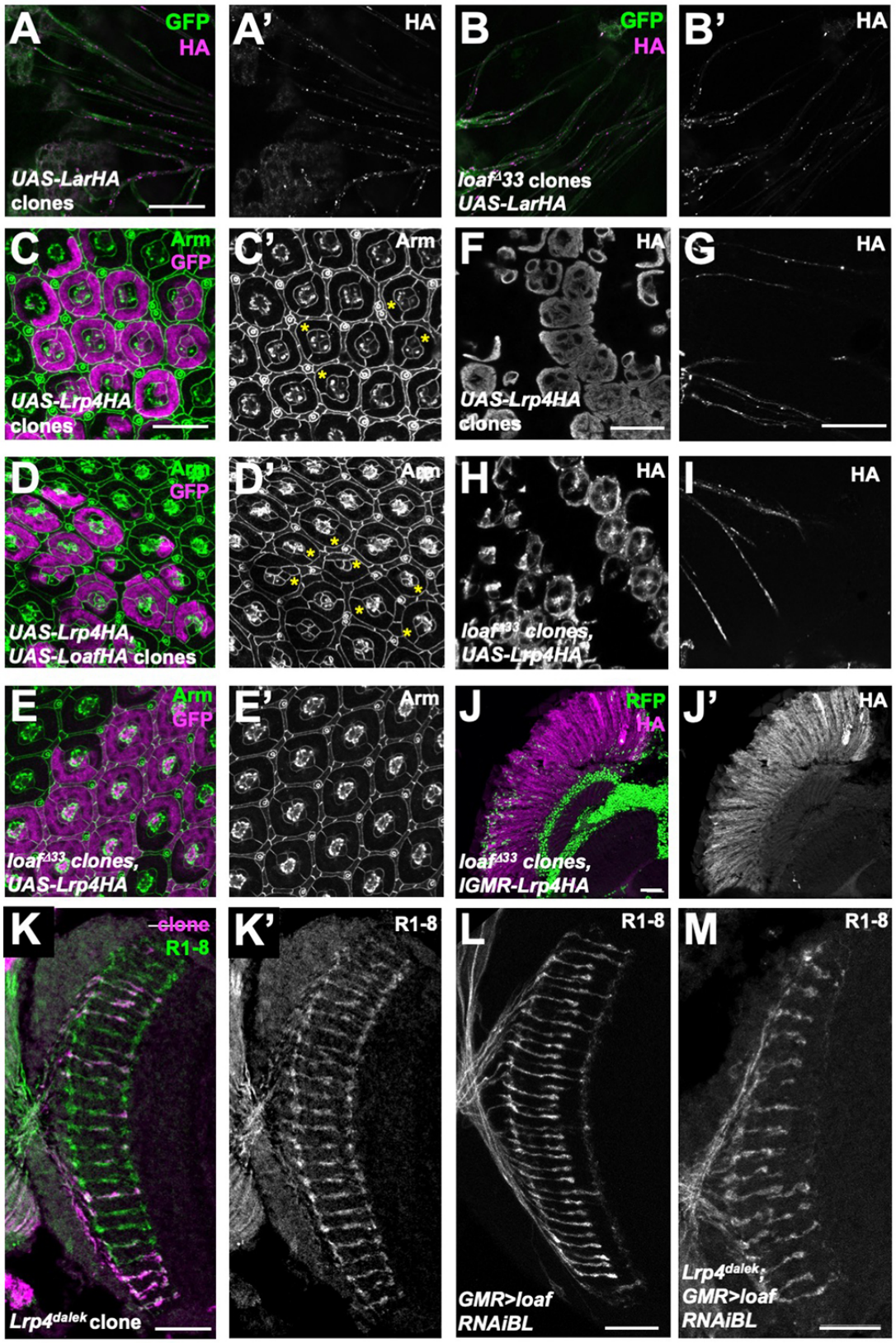

Douthit et al. Figure 7 – figure supplement 1

Figure 7 – figure supplement 1: Loaf does not visibly affect Lar or Lrp4 trafficking. (A, B) photoreceptor axons from clones in 42 h APF retinas positively labeled with GFP, stained for GFP (green) and HA (A', B, magenta in A, B). (A) wild type clones expressing *UAS-LarHA* with *lGMR-GAL4*; (B) *loaf*$^{\Delta 33}$ clones in which *UAS-LarHA* is expressed with *lGMR-GAL4*. Lar is transported into axons in wild type or *loaf* mutant photoreceptors. (C-E) 42 h APF retinas in which clones are positively labeled with GFP, stained for GFP (magenta) and Arm (C'-E', green in C-E). (C) clones expressing *UAS-Lrp4* with *lGMR-GAL4*; (D) clones expressing *UAS-Lrp4* and *UAS-LoafHA* with *lGMR-GAL4*; (E) *loaf*$^{\Delta 33}$ clones in which *UAS-Lrp4HA* is expressed with *lGMR-GAL4*. The ordered lattice structure of cone and pigment cells at the apical surface of the retina shows abnormalities (asterisks) when Lrp4 is overexpressed. These are more severe with Loaf coexpression and rescued in *loaf* mutant clones. (F-I) 42h APF pupal retinas in which *UAS-Lrp4HA* is expressed with *lGMR-GAL4* in wild type clones (F, G) or *loaf*$^{\Delta 33}$ mutant clones (H,I), stained for HA. (F, H) show photoreceptor cell bodies and (G, I) show their axons. Lrp4 is transported into axons in *loaf* mutant clones, but has a different appearance in cell bodies. (J) cryostat section of an adult head in which *UAS-Lrp4HA* is expressed in all cells with *lGMR-GAL4*, stained for HA (J', magenta in J). *loaf*$^{\Delta 33}$ clones are marked by the absence of RFP (green). The level of Lrp4 protein is unaffected by loss of *loaf*. (K-M) cryostat sections of adult heads stained for Chp (K', L, M, green in K) and GFP to positively label clones (magenta in K). (K) *Lrp4*^{dalek} clones do not show R7 mistargeting. (L, M) *GMR-GAL4* driving *UAS-loaf RNAiBL* causes R7 mistargeting in an otherwise wild type background (L) and in an *Lrp4*^{dalek} background (M). Scale bars, 20 μm.

mistargeting even in an *Lrp4* null mutant background (Figure 7 - figure supplement 1L, M). These results show that Loaf can affect the function of cell surface proteins, and suggest that it could act by regulating Lrp4 and/or other cell surface molecules that act as a readout of its levels to enable matching between R7 and its postsynaptic partners.

Discussion

Tm5a/b and Dm9 cells are involved in R7 targeting

The layered arrangement of neuronal processes in the medulla makes R7 axon targeting a sensitive model system in which to elucidate how growth cones select the correct postsynaptic partners. However, it has not been clear which cells are responsible for retaining R7 axons in the M6 layer. The RPTP Lar, which forms a hub for the assembly of presynaptic structures through the adaptor protein Liprin-α (Bomkamp et al., 2019, Hofmeyer et al., 2006, Choe et al., 2006, Takahashi and Craig, 2013), acts in R7 to stabilize filopodia in the M6 layer by promoting synapse formation (Maurel-Zaffran et al., 2001, Clandinin et al., 2001, Ozel et al., 2019). Although Lar family RPTPs can recognize a variety of ligands (Han et al., 2016), the ligand involved in R7 targeting and its cellular source remain unknown (Hofmeyer and Treisman, 2009). One candidate is Ncad, which is required at an early stage of development in both R7 and medulla neurons, but its widespread expression has made it difficult to determine which neurons are responsible for R7 synapse stabilization (Lee et al., 2001, Ting et al., 2005, Yonekura et al., 2007, Ozel et al., 2015). Lar overexpression can rescue the loss of *loaf*, suggesting that both Loaf and Lar act by stabilizing synaptic contacts.

R7 cells form numerous synapses with Dm8 interneurons, which are essential for ultraviolet spectral preference (Gao et al., 2008, Takemura et al., 2013) and fall into two classes that are postsynaptic to either yR7 or pR7 cells (Carrillo et al., 2015). Each R7 subtype promotes the survival of the class of Dm8 cells with which it synapses (Courgeon and Desplan, 2019, Menon et al., 2019). However, it is not known whether R7 relies on Dm8 for targeting or survival information; the Dm8 dendrites that remain in the absence of R7 cells still project to the M6 layer (Courgeon and Desplan, 2019). Many synapses between R7 and Dm8 also include the projection neurons Tm5a (yR7) or Tm5b (pR7) as a second postsynaptic element (Gao et al., 2008, Takemura et al., 2015, Menon et al., 2019). In addition, Dm9 interneurons are both pre- and postsynaptic to R7 and mediate center-surround inhibition, similarly to horizontal cells in the mammalian retina (Takemura et al., 2013, Takemura et al., 2015, Heath et al., 2020). Our data imply that the level of Loaf in Tm5a/b and Dm9 is more important for R7 targeting than its level in Dm8, suggesting that these cells may determine the stability of R7 contacts in the M6 layer. However, we cannot rule

out the possibility that the drivers we used to express Loaf in Dm8 did not cause a phenotype because the level or timing of expression was not optimal.

Matching levels of Loaf in pre- and postsynaptic cells may stabilize synapses

It is striking that the presence or absence of Loaf seems to be less significant than a difference in its level in R7 relative to its postsynaptic partners. In *loaf* mutants, redundant mechanisms must stabilize R7 terminals in the M6 layer. Synapses may not form entirely normally in these conditions, as *loaf* mutants show a reduced sensitivity to ultraviolet light when compared to isogenic controls (C.-H. Lee, pers. comm.). However, R7 mistargeting is much more striking when *loaf* is absent from photoreceptors, but present in the brain. We were able to reproduce this mistargeting by expressing *loaf* only in subsets of neurons in the brain that include postsynaptic partners of R7. The most parsimonious explanation for this is that a mismatch in the levels of Loaf between R7 and its partners results in mistargeting. A similar phenomenon was observed for Klingon, which affects synapse formation when removed from either R7 or glial cells, but not when removed from both simultaneously (Shimozono et al., 2019). Matching pre- and postsynaptic levels are also important for the *Drosophila* Teneurin proteins to promote synapse formation (Mosca et al., 2012, Hong et al., 2012). The type of matching we observe for Loaf, in which the presence of a protein in only one of the two cells inhibits synapse formation more strongly than its absence from both, is well suited to refining synaptic specificity by eliminating inappropriate connections.

Interestingly, Loaf matching seems to be asymmetric; mistargeting results if R7 has less Loaf than the postsynaptic cell, but not if the postsynaptic cell has less Loaf than R7. It is possible that matching in some way neutralizes the activity of Loaf, or of a cell surface molecule regulated by Loaf, and that an excess of this molecule on the postsynaptic cell prevents R7 from initiating or stabilizing synapses. However, the asymmetry could also reflect the presence of Loaf in multiple postsynaptic cells; loss of *loaf* from only one cell type may not be sufficient to disrupt R7 targeting. An alternative hypothesis that we cannot exclude is that R7 and another cell type use Loaf to compete for a ligand or for physical space in the M6 layer, so that the R7 terminal remains in M3 if it has less Loaf than its competitor. In the absence of drivers that are both early enough to precede

synapse formation and specific enough to express Loaf in only one cell type, it is difficult to definitively distinguish the matching and competition models.

Loaf may control the trafficking of a cell surface molecule

Our results suggest that Loaf may not itself act as a cell surface adhesion molecule. When epitope-tagged or untagged forms of Loaf are overexpressed in photoreceptors or cultured cells, they primarily localize to intracellular vesicles that include endosomes. In addition, they do not induce cell aggregation, arguing against a homophilic adhesion function of the low levels present on the cell surface. CUB domains are present in a variety of functionally distinct proteins, and are thought to bind protein ligands, sometimes in combination with calcium ions (Gaboriaud et al., 2011). Some CUB domain proteins are involved in endocytosis of other molecules (Moestrup and Verroust, 2001, Xu and Wang, 2016), while members of the Neuropilin and Tolloid-like (Neto) family of CUB-LDL proteins are required for the normal localization and activity of glutamate receptors and other postsynaptic proteins (Sheng et al., 2015, Kim et al., 2012, Zheng et al., 2004, Ramos et al., 2015). It is thus possible that Loaf controls the level of another protein on the cell surface by mediating its trafficking or endocytosis. The endosomal protein Commissureless functions in this manner, by trafficking the Roundabout axon guidance receptor directly from the Golgi to endosomes so that it does not reach the cell surface (Keleman et al., 2002). Differences in Neurexin levels between axons and dendrites are also dependent on endocytosis and sorting (Ribeiro et al., 2019), and trafficking of synaptic adhesion molecules in general is highly regulated (Ribeiro et al., 2018).

Consistent with this model, we found that loss or gain of Loaf affects the activity of coexpressed Lrp4, a presynaptic organizer in the olfactory system that has postsynaptic functions at mammalian neuromuscular junctions (Mosca et al., 2017, Yumoto et al., 2012). However, Lrp4 alone cannot explain the effects of Loaf, as removing *loaf* from photoreceptors still affects R7 targeting in an *Lrp4* null mutant. Loaf may act through a protein similar to Lrp4, or through a combination of proteins. Alternatively, it is possible that under some conditions, perhaps in the presence of other interacting proteins, Loaf itself can reach the cell surface and function there. Some synaptic organizing molecules are transported to axons in lysosome-related vesicles and secreted in a regulated manner (Vukoja et al., 2018, Ibata et al., 2019, Arantes and Andrews,

2006). Further study of the mechanism of Loaf action will provide insight into the cellular mechanisms that enable synapses to be constructed and stabilized on the appropriate cells as neural circuits develop.

Materials and Methods

Fly stocks and genetics

Fly stocks used were *Rh5-GFP* (Bloomington *Drosophila* Stock Center [BDSC] #8600); Rh6-GFP (BDSC #7461); *22E09-LexA*, *LexAop-myrTomato*; *GMR-GAL4* (Pecot et al., 2013); *ey3.5-FLP*, *Act>CD2>GAL4* (BDSC #35542 and #4780); *lGMR-GAL4* (BDSC #8605); *UAS-loaf RNAiBL P{TRiP.JF03040}attP2* (BDSC #28625); *UAS-loaf RNAiKK P{KK112220}VIE-260B* (Vienna *Drosophila* Resource Center [VDRC] #102704); *UAS-dcr2* (BDSC #24650); *panR7-lacZ* (Hofmeyer et al., 2006); *nos-Cas9* (BDSC #54591); *UAS-Cas9-P2* (BDSC #58986); *DIP-γ-GAL4* (Carrillo et al., 2015); *tj-GAL4*^{NP1624} (Kyoto Stock Center #104055); *drf-GAL4* (Brody et al., 2012); *Mi{PT-GFSTF.1}CG6024*$^{MI00316\text{-}GFSTF.1}$ (BDSC #64464); *ap*^{md544}*-GAL4* (BDSC #3041); *ChAT-GAL4* (BDSC #6798); *repo-GAL4* (BDSC #7415); *hth-GAL4* (Wernet et al., 2003); *bsh-GAL4* (Hasegawa et al., 2011); *Vsx-GAL4* (BDSC #29031); *VGlut-GAL4* (BDSC #26160); *GMR9D03-GAL4* (BDSC #40726); GH146-GAL4 (BDSC #30026); *dve*^{NP3428}*-GAL4* (Kyoto Stock Center #113273); *vg-GAL4* (Neumann and Cohen, 1996); *ort*^{C1a}*-GAL4* (BDSC #56519); *ort*^{C2b}*-GAL4* (Ting et al., 2014); *GMR64H01-GAL4* (BDSC #39322); *UAS-Lar-HA* (Hofmeyer and Treisman, 2009); *UAS-Lrp4-HA*; *Lrp4*^{dalek} (Mosca et al., 2017); *GMR9D03-DBD* (BDSC #68766); GMR38H04-AD (BDSC #75758); *MCFO-1* (Nern et al., 2015) and *TSG101*^{2} (Moberg et al., 2005).

loaf mutant clones and *loaf* mutant clones overexpressing other proteins were generated using *ey3.5-FLP*, *UAS-CD8GFP*; *lGMR-GAL4*; *FRT80*, *tub-GAL80*. Clones in which specific cell types were labeled were generated by crossing *ort*^{C2b}*-GAL4* (or other GAL4 lines); *FRT80* (or *FRT80, loaf*$^{\Delta 33}$) to *hs-FLP122, UAS-CD8GFP; FRT80, tub-GAL80*. Overexpression clones were generated by crossing *UAS-Loaf-HA* (or *UAS-Loaf*, *UAS-Lar-HA* or *UAS-Lrp4-HA*); *FRT82* to *ey3.5-FLP, UAS-CD8GFP; lGMR-GAL4; FRT82, tub-GAL80*. *loaf* mutant clones in a background of Lrp4 overexpression were generated by crossing *UAS-Lrp4HA; lGMR-GAL4*, *FRT80, loaf*$^{\Delta 33}$ to *eyFLP; FRT80, ubi-RFP*. *Lrp4* mutant clones were generated using *ey-FLP, tub-GAL80, FRT19; lGMR-GAL4, UAS-CD8-GFP*. To restore Loaf to specific cell types in a *loaf* mutant background, *tj-GAL4* (or other GAL4 lines); *loaf*$^{\Delta 33}$*/SM6-TM6B* was crossed to *UAS-Loaf-HA, UAS-myrTomato; loaf*$^{\Delta 33}$*/SM6-TM6B* or to *UAS-Loaf-HA; panR7-lacZ*, *loaf*$^{\Delta 33}$*/SM6-TM6B*. GAL4 lines on the third chromosome were recombined with *loaf*$^{\Delta 3}$ and recombinants carrying *loaf* were identified by PCR, except for GAL4

lines inserted at the *attP2* site, which is very close to *loaf*. In these cases, new *loaf* alleles were directly introduced by CRISPR onto the GAL4 chromosome using *nos-Cas9* and our transgenic *loaf sgRNA* flies, and identified by PCR.

Immunohistochemistry

Adult heads were dissected in cold 0.1 M sodium phosphate buffer (PB) pH 7.4, fixed in 4% formaldehyde in PB for 4 h at 4°C and washed in PB. Heads were then submerged in a sucrose gradient (5%, 10%, 20%) and left in 25% sucrose overnight at 4°C for cryoprotection. Heads were then embedded in OCT tissue freezing medium and frozen in dry ice/ethanol, and 12 μm sections were cut on a cryostat. Sections were post-fixed in 0.5% formaldehyde in PB for 30 min at room temperature and washed three times in PB with 0.1% Triton (PBT) before incubation with primary antibodies overnight at 4°C. Sections were washed 4 times for 20 min with PBT and incubated with secondary antibodies for 2 h at room temperature. Sections were washed again 4 times 20 min before mounting in Fluoromount-G (Southern Biotech).

Pupal and adult whole brains were fixed in 4% paraformaldehyde in PBS for 30 min at room temperature, washed 3 times for 10 min in PBST (PBS + 0.4% Triton-X 100) and blocked in PBST + 10% donkey serum prior to incubation with primary antibodies overnight at 4°C. Samples were washed in PBST 3 times for at least 1 hour each and incubated with secondary antibodies for 2.5 hours at room temperature. Samples were washed 3 times for 20 min in PBST and once in PBS before mounting in SlowFade Gold AntiFade reagent (Life Technologies) on bridge slides. Pupal retinas were fixed in 4% paraformaldehyde in PBS for 30 min on ice, washed for 15 min in PBT and incubated with primary antibodies overnight at 4°C. Retinas were washed 3 times for 5 min with PBT, incubated with secondary antibodies for 2 h at 4°C and washed again 3 times for 5 min before mounting in 80% glycerol in PBS. Confocal images were collected with Leica SP8 and Zeiss LSM510 confocal microscopes.

The primary antibodies used were mouse anti-Chp (1:50; Developmental Studies Hybridoma Bank [DSHB] 24B10), chicken anti-GFP (1:400; Life Technologies), rat anti-HA (1:50; Roche 3F10), rabbit anti-β galactosidase (1:100, MP Bio), rat anti-Ncad (1:50; DSHB), rabbit anti-dsRed (1:500; Living Color), guinea pig anti-Loaf (1:400, Proteintech), mouse anti-Cnx99A (1:10,

DSHB 6-2-1), mouse anti-Hrs (1:10, DSHB 27-4), mouse anti-Rab7 (1:10, DSHB), rabbit anti-ATP6V1B1 (Vha55; 1:200, Abgent), rabbit anti-Arl8 (1:200; DSHB), rat anti-Elav (1:100, DSHB), mouse anti-Dac (1:100; DSHB mAbdac1-1), mouse anti-Notch (1:10; DSHB C17.9C6), mouse anti-Arm (1:10; DSHB N2 7A1), sheep anti-GFP (1:200, Bio-rad #4745-1051), rabbit anti-RFP (1:500; MBL International #PM005), rabbit anti-V5 (1:1000; Abcam ab9116), mouse anti-FLAG (1:500, Sigma F3165), mouse anti-Dac (1:40; DSHB mAbdac2-3), rabbit anti-Bsh (1:1800; Ozel et al., under review), guinea pig anti-Runt (1:600; GenScript), and guinea pig anti-Otd (1:1000;GenScript). Rhodamine-phalloidin (Invitrogen R415) was used at 1:20. The Loaf polyclonal antibody was made by Proteintech using the cytoplasmic domain (aa 292-378) as an antigen. Guinea pig anti-serum was affinity purified. Guinea pig anti-Otd and guinea pig anti-Runt were made by GenScript using the full-length proteins as antigens. Secondary antibodies (Jackson Immunoresearch and Life Technologies) were coupled to the fluorochromes Cy3, Alexa Fluor 488, or Alexa Fluor 647.

Quantifications

To quantify the R7 targeting defect, fluorescent image stacks of 12-μm adult head sections labeled for *glass-lacZ*, *Rh3/4-lacZ*, or anti-24B10 were gathered in 0.5-μm steps. Maximum intensity projections were obtained and quantified by an observer blinded to their genotypes. Termini projecting beyond the R8 layer were counted as “R7 correctly targeted” and those stopping in the R8 layer were counted as “R7 incorrectly targeted.” Termini in the R8 layer were counted as total cartridge number per section. The percentage of mistargeting R7s was calculated for each section, except that when the phenotype was scored in photoreceptor clones, the percentage was calculated from all mistargeting R7 axons within clones from all sections. To quantify defects in UAS-LRP4 clones, GFP-labelled R7 termini that contacted each other in the M3 layer were counted as “M3 clumping”, while termini hyperfasciculating in the M6 layer were counted as “M6 clumping.” Three termini contacting each other were counted as two instances of M3 or M6 clumping depending on in which layer the clumps resided. GFP-labelled R7 termini that extended past the M6 layer were counted as “overshooting.” A terminus that extended past the M6 layer and turned to contact another clone was counted both as “M6 clumping” and “overshooting.” The percentage of R7s belonging to each of these groups was calculated from all the R7 clones within each section.

To quantify cell aggregates in S2 cell culture experiments, fluorescent image stacks from fixed cells that had been labeled for GFP and HA were gathered in 0.5-μm steps. Each image was examined for GFP positive (control) or GFP and HA positive (Sdk and Loaf) cells that contacted each other as aggregates. The number of cells in each aggregate was counted for each image. To measure intracellular colocalization, single confocal slices were processed with a median filter with neighborhood of 1 in ImageJ and each channel was linear contrast enhanced to spread values evenly from 0 to 255. A rectangular ROI was drawn around the central region of a single ommatidium and ImageJ was used to calculate Pearson's correlation coefficient on each region with pixel intensity above a threshold of 16 out of a range of 255, to eliminate background.

Western blotting

To extract proteins, adult heads were dissected and frozen on dry ice, and then homogenized in Laemmli buffer (4% SDS, 20% glycerol, 120 mM Tris-Cl pH 6.8, 0.02% bromophenol blue, 10% beta-mercaptoethanol). Samples were heated at 95°C for 5 min and loaded onto a SDS-PAGE gel. Gels were run first at 80 volts for 20 min, then 100 volts for the remainder of the time and transferred onto nitrocellulose membranes (Bio-rad) for one hour at 100 volts. Membranes were washed for 5 min in TBST (20mM Tris (pH 7.6), 136 mMNaCl, 0.2% Tween-20), and blocked in 5% low-fat milk in TBST solution for one hour. Membranes were incubated overnight with primary antibody in TBST with 5% milk at 4°C, washed 3 times for 10 minutes in TBST and incubated in horseradish peroxidase-conjugated secondary antibodies (1:10,000; Jackson ImmunoResearch) at room temperature in TBST with 5% milk for 2 h. Membranes were washed 3 times for 10 min in TBST and once for 10 min in TBS. Enhanced chemiluminescence (Thermo SuperSignal WestPico) was used to develop the blots. Primary antibodies used were guinea pig anti-Loaf (1:1000, Proteintech) and mouse anti ß-tubulin (1:10,000; Sigma, T4026).

Cloning and transgenic lines

UAS-Loaf-FLAG-HA is clone UFO07678 (*Drosophila* Genomics Resource Center). UAS-Loaf was cloned by inserting an Nhe I/Xba I fragment of clone UFO07678 into the Xba I site of pUAST-attB. Both constructs were integrated into the VK1 PhiC31 site at position 59D3. The *loaf* sgRNA

sequences GCTGGTGATTACGTCGGTGA (*loaf* gRNA 1) and TGCGGGACCATCCGGGTACC (*loaf* gRNA 2) identified on www.flyrnai.org/crispr2 were made with gene synthesis in pUC57 (GenScript) and cloned into pCFD4 (Port et al., 2014) by Gibson assembly. The construct was integrated into the attP40 site at 25C6. These flies were crossed to *nos*-Cas9 flies to make germline mosaic flies. The progeny of these flies were crossed to balancer flies and screened by PCR using primers outside the expected deletion (CGCACGAACTTTGTGACACT and CTCAAGTCAATCGGTCCTTCC). Injections and screening of transgenic flies were carried out by Genetivision.

S2 cell culture and aggregation assay

S2 cells were grown in Schneider's *Drosophila* Medium (GIBCO Invitrogen) with 10% heat inactivated fetal bovine serum and 50 units/ml penicillin-50 g/ml streptomycin (GIBCO Invitrogen) at 25°C. Cells were spun down and resuspended in PBS. Poly-L-lysine-treated slides were covered with 0.1-0.2 ml of the cell suspension. Cells were fixed for 10 min at room temperature with 4% paraformaldehyde, permeabilized for 15 min with 0.2% PBT, then blocked with 10% normal donkey serum. Slides were incubated with primary antibodies overnight at 4°C in a humid chamber, washed 4 times with PBS, and incubated with secondary antibody at room temperature for 1-2 hours. Samples were washed 3 times with PBS before mounting with Vectashield (Vector Labs). Pictures were collected on a Leica SP8 confocal microscope.

For aggregation assays, S2 cells were pelleted 48 hours after transient transfection using Effectene Transfection Reagent (Qiagen) and washed in fresh medium. 2.5 ml of cells at a concentration of 4 x 10^6 cells/ml were rocked at 50 rpm for at least 3 hours. Plates were then analyzed for the presence of cell aggregates. Pictures were collected on a Zeiss AxioZoom microscope. All cell culture experiments were repeated three times.

Acknowledgements

We thank Steve Cohen, Max Courgeon, Chi-Hon Lee, Ken Moberg, Tim Mosca, Larry Zipursky, the Bloomington *Drosophila* Stock Center, the Vienna *Drosophila* Resource Center, the Kyoto Stock Center, the *Drosophila* Genomics Resource Center and the Developmental Studies Hybridoma Bank for fly stocks and reagents, and Flybase for invaluable information. We thank Michael Cammer of the NYU Langone Microscopy Laboratory, which is supported by grant P30CA016087, for help with quantifying colocalization. We are grateful to Justine Oyallon for her contributions to the early stages of the project, and to Hui Hua Liu and DanQing He for technical assistance. The manuscript was improved by the critical comments of Hongsu Wang. This work was supported by NIH grants R01GM089799 and R01NS112211 to J.E.T. and by fellowship F31EY025568 to J.D.

Competing interests: The authors declare no competing interests.

References

ARANTES, R. M. & ANDREWS, N. W. 2006. A role for synaptotagmin VII-regulated exocytosis of lysosomes in neurite outgrowth from primary sympathetic neurons. *J Neurosci,* 26**,** 4630-7.

ASTIGARRAGA, S., DOUTHIT, J., TARNOGORSKA, D., CREAMER, M. S., MANO, O., CLARK, D. A., MEINERTZHAGEN, I. A. & TREISMAN, J. E. 2018. *Drosophila* Sidekick is required in developing photoreceptors to enable visual motion detection. *Development,* 145, pii: dev158246.

BAZIGOU, E., APITZ, H., JOHANSSON, J., LOREN, C. E., HIRST, E. M., CHEN, P. L., PALMER, R. H. & SALECKER, I. 2007. Anterograde Jelly belly and Alk receptor tyrosine kinase signaling mediates retinal axon targeting in *Drosophila*. *Cell,* 128**,** 961-75.

BOMKAMP, C., PADMANABHAN, N., KARIMI, B., GE, Y., CHAO, J. T., LOEWEN, C. J. R., SIDDIQUI, T. J. & CRAIG, A. M. 2019. Mechanisms of PTPsigma-mediated presynaptic differentiation. *Front Synaptic Neurosci,* 11**,** 17.

BRODY, T., YAVATKAR, A. S., KUZIN, A., KUNDU, M., TYSON, L. J., ROSS, J., LIN, T. Y., LEE, C. H., AWASAKI, T., LEE, T. & ODENWALD, W. F. 2012. Use of a *Drosophila* genome-wide conserved sequence database to identify functionally related cis-regulatory enhancers. *Dev Dyn,* 241**,** 169-89.

CARRILLO, R. A., OZKAN, E., MENON, K. P., NAGARKAR-JAISWAL, S., LEE, P. T., JEON, M., BIRNBAUM, M. E., BELLEN, H. J., GARCIA, K. C. & ZINN, K. 2015. Control of synaptic connectivity by a network of *Drosophila* IgSF cell surface proteins. *Cell,* 163**,** 1770-1782.

CHOE, K. M., PRAKASH, S., BRIGHT, A. & CLANDININ, T. R. 2006. Liprin-alpha is required for photoreceptor target selection in *Drosophila*. *Proc Natl Acad Sci U S A,* 103**,** 11601-6.

CLANDININ, T. R., LEE, C. H., HERMAN, T., LEE, R. C., YANG, A. Y., OVASAPYAN, S. & ZIPURSKY, S. L. 2001. *Drosophila* LAR regulates R1-R6 and R7 target specificity in the visual system. *Neuron,* 32**,** 237-48.

COURGEON, M. & DESPLAN, C. 2019. Coordination between stochastic and deterministic specification in the *Drosophila* visual system. *Science,* 366, pii: eaay6727.

CULI, J., SPRINGER, T. A. & MANN, R. S. 2004. Boca-dependent maturation of beta-propeller/EGF modules in low-density lipoprotein receptor proteins. *EMBO J,* 23**,** 1372-80.

DAVIS, F. P., NERN, A., PICARD, S., REISER, M. B., RUBIN, G. M., EDDY, S. R. & HENRY, G. L. 2020. A genetic, genomic, and computational resource for exploring neural circuit function. *Elife,* 9, pii: e50901.

ERCLIK, T., LI, X., COURGEON, M., BERTET, C., CHEN, Z., BAUMERT, R., NG, J., KOO, C., ARAIN, U., BEHNIA, R., DEL VALLE RODRIGUEZ, A., SENDEROWICZ, L., NEGRE, N., WHITE, K. P. & DESPLAN, C. 2017. Integration of temporal and spatial patterning generates neural diversity. *Nature,* 541**,** 365-370.

FREEMAN, M. 1996. Reiterative use of the EGF receptor triggers differentiation of all cell types in the *Drosophila* eye. *Cell,* 87**,** 651-60.

GABORIAUD, C., GREGORY-PAURON, L., TEILLET, F., THIELENS, N. M., BALLY, I. & ARLAUD, G. J. 2011. Structure and properties of the Ca(2+)-binding CUB domain, a widespread ligand-recognition unit involved in major biological functions. *Biochem J,* 439**,** 185-93.

GAO, S., TAKEMURA, S. Y., TING, C. Y., HUANG, S., LU, Z., LUAN, H., RISTER, J., THUM, A. S., YANG, M., HONG, S. T., WANG, J. W., ODENWALD, W. F., WHITE, B. H., MEINERTZHAGEN, I. A. &

LEE, C. H. 2008. The neural substrate of spectral preference in *Drosophila*. *Neuron,* 60**,** 328-42.

GILBERT, J. & MAN, H. Y. 2017. Fundamental elements in autism: from neurogenesis and neurite growth to synaptic plasticity. *Front Cell Neurosci,* 11**,** 359.

HAKEDA-SUZUKI, S., TAKECHI, H., KAWAMURA, H. & SUZUKI, T. 2017. Two receptor tyrosine phosphatases dictate the depth of axonal stabilizing layer in the visual system. *Elife,* 6, pii: e31812.

HAN, K. A., JEON, S., UM, J. W. & KO, J. 2016. Emergent synapse organizers: LAR-RPTPs and their companions. *Int Rev Cell Mol Biol,* 324**,** 39-65.

HASEGAWA, E., KITADA, Y., KAIDO, M., TAKAYAMA, R., AWASAKI, T., TABATA, T. & SATO, M. 2011. Concentric zones, cell migration and neuronal circuits in the *Drosophila* visual center. *Development,* 138**,** 983-93.

HEATH, S. L., CHRISTENSON, M. P., ORIOL, E., SAAVEDRA-WEISENHAUS, M., KOHN, J. R. & BEHNIA, R. 2020. Circuit mechanisms underlying chromatic encoding in *Drosophila* photoreceptors. *Curr Biol,* 30**,** 264-275.

HOFMEYER, K., MAUREL-ZAFFRAN, C., SINK, H. & TREISMAN, J. E. 2006. Liprin-alpha has LAR-independent functions in R7 photoreceptor axon targeting. *Proc Natl Acad Sci U S A,* 103**,** 11595-600.

HOFMEYER, K. & TREISMAN, J. E. 2009. The receptor protein tyrosine phosphatase LAR promotes R7 photoreceptor axon targeting by a phosphatase-independent signaling mechanism. *Proc Natl Acad Sci U S A,* 106**,** 19399-404.

HOLBROOK, S., FINLEY, J. K., LYONS, E. L. & HERMAN, T. G. 2012. Loss of *syd-1* from R7 neurons disrupts two distinct phases of presynaptic development. *J Neurosci,* 32**,** 18101-11.

HONG, W., MOSCA, T. J. & LUO, L. 2012. Teneurins instruct synaptic partner matching in an olfactory map. *Nature,* 484**,** 201-7.

IBATA, K., KONO, M., NARUMI, S., MOTOHASHI, J., KAKEGAWA, W., KOHDA, K. & YUZAKI, M. 2019. Activity-dependent secretion of synaptic organizer Cbln1 from lysosomes in granule cell axons. *Neuron,* 102**,** 1184-1198.

KARUPPUDURAI, T., LIN, T. Y., TING, C. Y., PURSLEY, R., MELNATTUR, K. V., DIAO, F., WHITE, B. H., MACPHERSON, L. J., GALLIO, M., POHIDA, T. & LEE, C. H. 2014. A hard-wired glutamatergic circuit pools and relays UV signals to mediate spectral preference in *Drosophila*. *Neuron,* 81**,** 603-615.

KELEMAN, K., RAJAGOPALAN, S., CLEPPIEN, D., TEIS, D., PAIHA, K., HUBER, L. A., TECHNAU, G. M. & DICKSON, B. J. 2002. Comm sorts Robo to control axon guidance at the *Drosophila* midline. *Cell,* 110**,** 415-27.

KIM, Y. J., BAO, H., BONANNO, L., ZHANG, B. & SERPE, M. 2012. *Drosophila* Neto is essential for clustering glutamate receptors at the neuromuscular junction. *Genes Dev,* 26**,** 974-87.

KONSTANTINIDES, N., KAPURALIN, K., FADIL, C., BARBOZA, L., SATIJA, R. & DESPLAN, C. 2018. Phenotypic convergence: distinct transcription factors regulate common terminal features. *Cell,* 174**,** 622-635.

KULKARNI, A., ERTEKIN, D., LEE, C. H. & HUMMEL, T. 2016. Birth order dependent growth cone segregation determines synaptic layer identity in the *Drosophila* visual system. *Elife,* 5**,** e13715.

LEE, C. H., HERMAN, T., CLANDININ, T. R., LEE, R. & ZIPURSKY, S. L. 2001. N-cadherin regulates target specificity in the *Drosophila* visual system. *Neuron,* 30**,** 437-50.

LI, X., ERCLIK, T., BERTET, C., CHEN, Z., VOUTEV, R., VENKATESH, S., MORANTE, J., CELIK, A. & DESPLAN, C. 2013. Temporal patterning of *Drosophila* medulla neuroblasts controls neural fates. *Nature,* 498**,** 456-62.

MAUREL-ZAFFRAN, C., SUZUKI, T., GAHMON, G., TREISMAN, J. E. & DICKSON, B. J. 2001. Cell-autonomous and -nonautonomous functions of LAR in R7 photoreceptor axon targeting. *Neuron,* 32**,** 225-35.

MENON, K. P., KULKARNI, V., TAKEMURA, S. Y., ANAYA, M. & ZINN, K. 2019. Interactions between Dpr11 and DIP-gamma control selection of amacrine neurons in *Drosophila* color vision circuits. *Elife,* 8, e48935.

MOBERG, K. H., SCHELBLE, S., BURDICK, S. K. & HARIHARAN, I. K. 2005. Mutations in *erupted*, the *Drosophila* ortholog of mammalian *tumor susceptibility gene 101*, elicit non-cell-autonomous overgrowth. *Dev Cell,* 9**,** 699-710.

MOESTRUP, S. K. & VERROUST, P. J. 2001. Megalin- and cubilin-mediated endocytosis of protein-bound vitamins, lipids, and hormones in polarized epithelia. *Annu Rev Nutr,* 21**,** 407-28.

MOSCA, T. J., HONG, W., DANI, V. S., FAVALORO, V. & LUO, L. 2012. Trans-synaptic Teneurin signalling in neuromuscular synapse organization and target choice. *Nature,* 484**,** 237-41.

MOSCA, T. J., LUGINBUHL, D. J., WANG, I. E. & LUO, L. 2017. Presynaptic LRP4 promotes synapse number and function of excitatory CNS neurons. *Elife,* 6, e27347.

MOSES, K., ELLIS, M. C. & RUBIN, G. M. 1989. The *glass* gene encodes a zinc-finger protein required by *Drosophila* photoreceptor cells. *Nature,* 340**,** 531-6.

NAVAL-SANCHEZ, M., POTIER, D., HAAGEN, L., SANCHEZ, M., MUNCK, S., VAN DE SANDE, B., CASARES, F., CHRISTIAENS, V. & AERTS, S. 2013. Comparative motif discovery combined with comparative transcriptomics yields accurate targetome and enhancer predictions. *Genome Res,* 23**,** 74-88.

NERN, A., PFEIFFER, B. D. & RUBIN, G. M. 2015. Optimized tools for multicolor stochastic labeling reveal diverse stereotyped cell arrangements in the fly visual system. *Proc Natl Acad Sci U S A,* 112**,** E2967-76.

NEUMANN, C. J. & COHEN, S. M. 1996. A hierarchy of cross-regulation involving *Notch*, *wingless*, *vestigial* and *cut* organizes the dorsal/ventral axis of the *Drosophila* wing. *Development,* 122**,** 3477-85.

NEWSOME, T. P., ASLING, B. & DICKSON, B. J. 2000. Analysis of *Drosophila* photoreceptor axon guidance in eye-specific mosaics. *Development,* 127**,** 851-60.

OZEL, M. N., KULKARNI, A., HASAN, A., BRUMMER, J., MOLDENHAUER, M., DAUMANN, I. M., WOLFENBERG, H., DERCKSEN, V. J., KIRAL, F. R., WEISER, M., PROHASKA, S., VON KLEIST, M. & HIESINGER, P. R. 2019. Serial synapse formation through filopodial competition for synaptic seeding factors. *Dev Cell*, 50, 447-461.

OZEL, M. N., LANGEN, M., HASSAN, B. A. & HIESINGER, P. R. 2015. Filopodial dynamics and growth cone stabilization in Drosophila visual circuit development. *Elife,* 4, e10721.

PAPPU, K. S., MOREY, M., NERN, A., SPITZWECK, B., DICKSON, B. J. & ZIPURSKY, S. L. 2011. Robo-3-mediated repulsive interactions guide R8 axons during *Drosophila* visual system development. *Proc Natl Acad Sci U S A,* 108**,** 7571-6.

PECOT, M. Y., TADROS, W., NERN, A., BADER, M., CHEN, Y. & ZIPURSKY, S. L. 2013. Multiple interactions control synaptic layer specificity in the *Drosophila* visual system. *Neuron,* 77**,** 299-310.

PETROVIC, M. & HUMMEL, T. 2008. Temporal identity in axonal target layer recognition. *Nature,* 456**,** 800-3.

PLAZAOLA-SASIETA, H., FERNANDEZ-PINEDA, A., ZHU, Q. & MOREY, M. 2017. Untangling the wiring of the *Drosophila* visual system: developmental principles and molecular strategies. *J Neurogenet,* 31**,** 231-249.

PORT, F., CHEN, H. M., LEE, T. & BULLOCK, S. L. 2014. Optimized CRISPR/Cas tools for efficient germline and somatic genome engineering in *Drosophila*. *Proc Natl Acad Sci U S A,* 111**,** E2967-76.

RAMOS, C. I., IGIESUOROBO, O., WANG, Q. & SERPE, M. 2015. Neto-mediated intracellular interactions shape postsynaptic composition at the *Drosophila* neuromuscular junction. *PLoS Genet,* 11**,** e1005191.

RIBEIRO, L. F., VERPOORT, B. & DE WIT, J. 2018. Trafficking mechanisms of synaptogenic cell adhesion molecules. *Mol Cell Neurosci,* 91**,** 34-47.

RIBEIRO, L. F., VERPOORT, B., NYS, J., VENNEKENS, K. M., WIERDA, K. D. & DE WIT, J. 2019. SorCS1-mediated sorting in dendrites maintains neurexin axonal surface polarization required for synaptic function. *PLoS Biol,* 17**,** e3000466.

SCHWABE, T., BORYCZ, J. A., MEINERTZHAGEN, I. A. & CLANDININ, T. R. 2014. Differential adhesion determines the organization of synaptic fascicles in the *Drosophila* visual system. *Curr Biol,* 24**,** 1304-1313.

SELLECK, S. B. & STELLER, H. 1991. The influence of retinal innervation on neurogenesis in the first optic ganglion of *Drosophila*. *Neuron,* 6**,** 83-99.

SHENG, N., SHI, Y. S., LOMASH, R. M., ROCHE, K. W. & NICOLL, R. A. 2015. Neto auxiliary proteins control both the trafficking and biophysical properties of the kainate receptor GluK1. *Elife,* 4, e11682.

SHIMOZONO, M., OSAKA, J., KATO, Y., ARAKI, T., KAWAMURA, H., TAKECHI, H., HAKEDA-SUZUKI, S. & SUZUKI, T. 2019. Cell surface molecule, Klingon, mediates the refinement of synaptic specificity in the *Drosophila* visual system. *Genes Cells,* 24**,** 496-510.

TAKAHASHI, H. & CRAIG, A. M. 2013. Protein tyrosine phosphatases PTPdelta, PTPsigma, and LAR: presynaptic hubs for synapse organization. *Trends Neurosci,* 36**,** 522-34.

TAKEMURA, S. Y., BHARIOKE, A., LU, Z., NERN, A., VITALADEVUNI, S., RIVLIN, P. K., KATZ, W. T., OLBRIS, D. J., PLAZA, S. M., WINSTON, P., ZHAO, T., HORNE, J. A., FETTER, R. D., TAKEMURA, S., BLAZEK, K., CHANG, L. A., OGUNDEYI, O., SAUNDERS, M. A., SHAPIRO, V., SIGMUND, C., RUBIN, G. M., SCHEFFER, L. K., MEINERTZHAGEN, I. A. & CHKLOVSKII, D. B. 2013. A visual motion detection circuit suggested by *Drosophila* connectomics. *Nature,* 500**,** 175-81.

TAKEMURA, S. Y., XU, C. S., LU, Z., RIVLIN, P. K., PARAG, T., OLBRIS, D. J., PLAZA, S., ZHAO, T., KATZ, W. T., UMAYAM, L., WEAVER, C., HESS, H. F., HORNE, J. A., NUNEZ-IGLESIAS, J., ANICETO, R., CHANG, L. A., LAUCHIE, S., NASCA, A., OGUNDEYI, O., SIGMUND, C., TAKEMURA, S., TRAN, J., LANGILLE, C., LE LACHEUR, K., MCLIN, S., SHINOMIYA, A., CHKLOVSKII, D. B., MEINERTZHAGEN, I. A. & SCHEFFER, L. K. 2015. Synaptic circuits and their variations within different columns in the visual system of *Drosophila*. *Proc Natl Acad Sci U S A,* 112**,** 13711-6.

TING, C. Y., MCQUEEN, P. G., PANDYA, N., LIN, T. Y., YANG, M., REDDY, O. V., O'CONNOR, M. B., MCAULIFFE, M. & LEE, C. H. 2014. Photoreceptor-derived Activin promotes dendritic termination and restricts the receptive fields of first-order interneurons in *Drosophila*. *Neuron,* 81**,** 830-846.

TING, C. Y., YONEKURA, S., CHUNG, P., HSU, S. N., ROBERTSON, H. M., CHIBA, A. & LEE, C. H. 2005. *Drosophila* N-cadherin functions in the first stage of the two-stage layer-selection process of R7 photoreceptor afferents. *Development,* 132**,** 953-63.

TRIPLETT, J. W. & FELDHEIM, D. A. 2012. Eph and ephrin signaling in the formation of topographic maps. *Semin Cell Dev Biol,* 23**,** 7-15.

VAN BATTUM, E. Y., BRIGNANI, S. & PASTERKAMP, R. J. 2015. Axon guidance proteins in neurological disorders. *Lancet Neurol,* 14**,** 532-46.

VUKOJA, A., REY, U., PETZOLDT, A. G., OTT, C., VOLLWEITER, D., QUENTIN, C., PUCHKOV, D., REYNOLDS, E., LEHMANN, M., HOHENSEE, S., ROSA, S., LIPOWSKY, R., SIGRIST, S. J. & HAUCKE, V. 2018. Presynaptic biogenesis requires axonal transport of lysosome-related vesicles. *Neuron,* 99**,** 1216-1232.

WAGNER, T., DIECKMANN, M., JAEGER, S., WEGGEN, S. & PIETRZIK, C. U. 2013. Stx5 is a novel interactor of VLDL-R to affect its intracellular trafficking and processing. *Exp Cell Res,* 319**,** 1956-72.

WERNET, M. F., LABHART, T., BAUMANN, F., MAZZONI, E. O., PICHAUD, F. & DESPLAN, C. 2003. Homothorax switches function of *Drosophila* photoreceptors from color to polarized light sensors. *Cell,* 115**,** 267-79.

XU, Y. & WANG, T. 2016. CULD is required for rhodopsin and TRPL channel endocytic trafficking and survival of photoreceptor cells. *J Cell Sci,* 129**,** 394-405.

YOGEV, S. & SHEN, K. 2014. Cellular and molecular mechanisms of synaptic specificity. *Annu Rev Cell Dev Biol,* 30**,** 417-37.

YONEKURA, S., XU, L., TING, C. Y. & LEE, C. H. 2007. Adhesive but not signaling activity of *Drosophila* N-cadherin is essential for target selection of photoreceptor afferents. *Dev Biol,* 304**,** 759-70.

YUMOTO, N., KIM, N. & BURDEN, S. J. 2012. Lrp4 is a retrograde signal for presynaptic differentiation at neuromuscular synapses. *Nature,* 489**,** 438-42.

ZHANG, K. X., TAN, L., PELLEGRINI, M., ZIPURSKY, S. L. & MCEWEN, J. M. 2016. Rapid changes in the translatome during the conversion of growth cones to synaptic terminals. *Cell Rep,* 14**,** 1258-1271.

ZHENG, Y., MELLEM, J. E., BROCKIE, P. J., MADSEN, D. M. & MARICQ, A. V. 2004. SOL-1 is a CUB-domain protein required for GLR-1 glutamate receptor function in *C. elegans*. *Nature,* 427**,** 451-7.